1-1-2013

A raised OIS 3 sea level recorded in coastal sediments, southern Changjiang delta plain, China

Zhanghua Wang
East China Normal University

Brian G. Jones
University of Wollongong, briangj@uow.edu.au

Ting Chen
East China Normal University

Baocheng Zhao
Shanghai Geological Survey

Qing Zhan
Shanghai Geological Survey

A raised OIS 3 sea level recorded in coastal sediments, southern Changjiang delta plain, China

Abstract

The distribution of marine-influenced oxygen isotope stage (OIS) 5 to OIS 1 sediments was examined in several late Quaternary boreholes from the southern Changjiang (Yangtze) delta plain, China, using different dating methods including OSL, U-series, AMS 14C and paleomagnetism. Results demonstrate that coastal and estuarine deposition during OIS 5 and OIS 3 occurred throughout the study area. However, Holocene transgressive sediments were absent on the Taihu block. The burial depth of intertidal to subtidal sediment deposited during OIS 5e records 30-80 m subsidence caused by sediment compaction and tectonic movement since that time. However, coastal sediments formed during the late phase of OIS 3 were buried to a depth of ca. 6-15 m in the Taihu Lake area, while the burial depth increased eastward to ca. 45-60 m on the coastal plain. This phenomenon, combined with the distribution of Holocene marine strata, indicates at least 25-30 m uplift of the Taihu block since the end of OIS 3. We suggest that this uplift was mainly caused by the differential subsidence due to substantial amount of post-glacial deposition by the Changjiang and Huanghe Rivers on the continental shelf of east China marginal sea.

Keywords

OIS 3 sea level, differential subsidence, uplift of Taihu block, Changjiang coast, GeoQuest

Disciplines

Medicine and Health Sciences | Social and Behavioral Sciences

Publication Details

Wang, Z., Jones, B. G., Chen, T., Zhao, B. & Zhan, Q. (2013). A raised OIS 3 sea level recorded in coastal sediments, southern Changjiang delta plain, China. Quaternary Research, 79 (3), 424-438.

A raised OIS 3 sea level recorded in coastal sediments, southern Changjiang delta plain, China

Zhanghua Wang[a*], Brian G. Jones[b], Ting Chen[a], Baocheng Zhao[c], Qing Zhan[c]

[a] State Key Laboratory for Estuarine and Coastal Research, East China Normal University, Shanghai 200062, China

[b] School of Earth and Environmental Sciences, University of Wollongong, NSW 2522, Australia

[c] Shanghai Geological Survey, Shanghai 200072, China

* Corresponding author, Tel: 86 21 62232887; Fax: 86 21 62546441; email address: zhwang@geo.ecnu.edu.cn

Abstract

The distribution of marine influenced oxygen isotope stage (OIS) 5 to OIS 1 sediments were examined in several late Quaternary boreholes from the southern Changjiang (Yangtze) delta plain, China, using different dating methods including OSL, U-series, AMS ^{14}C and paleomagnetism. Results demonstrate that coastal and estuarine deposition during OIS 5 and OIS 3 occurred throughout the study area. However, Holocene transgressive sediments were absent on the Taihu block. The burial depth of intertidal to subtidal sediment deposited during OIS 5e records 30–80 m subsidence caused by sediment compaction and tectonic movement since that time. However, coastal sediments formed during the late phase of OIS 3 were buried to a depth of *c.* 6–15 m in the Taihu Lake area, while the burial depth increased remarkably eastward to *c.* 45–60 m on the coastal plain. This phenomenon, combined with the

distribution of Holocene marine strata, indicates at least 25–30 m uplift of the Taihu block since the end of OIS 3. We suggest that this uplift was mainly caused by the differential subsidence due to substantial amount of post-glacial deposition by the Changjiang and Huanghe Rivers on the continental shelf of east China marginal sea.

Keywords: OIS 3 sea level; differential subsidence; uplift of Taihu block; Changjiang coast

1. Introduction

The OIS 3 sea level has become the focus of recent research and different points of view exist from evidence supplied by oxygen isotopes of foraminifera in deep sea sediments, coral reefs, and coastal and shelf sediments (Chappell and Shackleton, 1986; Shackleton, 1987; Chappell et al., 1996; Chappell, 2002; Siddall et al., 2003; Hanebuth et al., 2006; Parham et al., 2007; Mallinson et al., 2008; Wright et al., 2009). For example, results from the east coast of North American revealed that the OIS 3 highstand could be at -25 m below present mean sea level (PMSL) after correction for glacio-isostatic adjustment (Mallinson et al., 2008; Wright et al., 2009). This contrasts significantly with heights of -35–-45 m estimated from the planktonic and benthonic oxygen isotope compositions in deep sea records (Shackleton, 1987; Siddall et al., 2003).

A subsiding coastal area like the Changjiang (Yangtze) delta is believed to have the potential to record sea level due not only to sensitivity of the coastal depositional environment to sea level change, but also to rapid sedimentation rates and a potential high resolution sedimentation record. Previous work in the delta and adjacent continental shelf reported OIS 3 sediments that indicate a relative sea level of up to *c.* -5 m below PMSL during late OIS 3

(Zhao et al., 2008). However, only two ^{14}C ages from organic-rich mud have been collected from previous boreholes ZK04 and 827 (Fig. 1a) around the Taihu Lake on the southern Changjiang delta plain where OIS 3 sediments are suggested to be present just below ground surface. Furthermore, Liu et al. (2009) indicated that the OIS 3 relative sea level ranged from -35±5 to -60±5 m or lower off the Yellow River delta in the Bohai Sea, China. Therefore, the previously reported highstand of OIS 3 needed to be re-examined with a more detailed chronological study and mechanism of the raised OIS 3 marine sediments for the Changjiang delta plain.

In this research, we recovered two late Quaternary boreholes, WJ and QP88 from the Taihu block (Fig. 1). We applied different dating methods including OSL (optically stimulated luminescence), U-series and AMS^{14}C dating (Tables 1–4), together with paleomagnetism to the sediments and mollusc shells from these two boreholes. Combining with our previous OSL and U-series dated boreholes SG7, FX and MFC (Fig. 1), this research examines the late Quaternary stratigraphy and sedimentary environment as well as constrains the chronology of late Pleistocene marine-influenced strata and relative sea level in the study area, to discuss possible reasons for sea level highstand during OIS 3 by comparing sedimentary records from the Changjiang delta with global data, especially that from the surrounding regions.

2. Geologic setting

The Changjiang delta, located on the eastern coast of China, is one of the most vulnerable coastal lowlands to the sea level rise in the world (Syvitski et al., 2009). The Changjiang River discharge sediment *c*. 460 Mt/yr into the river mouth during the late half

century of 20th and now sediment load has declined to less than 200 Mt/yr due to construction of reservoir in the upstream (Yang et al., 2011). The present morphology of the delta plain is dish-like, i.e., big lakes and depressions (0–2 m in elevation) in the centre surrounded by a higher coastal plain (3–5 m in elevation; Fig. 1a). There are several ridges of chenier formed during the mid-Holocene at the east boundary between the Taihu lacustrine and coastal plain. However, numerous boreholes proved a morphological high of the lacustrine plain, the Taihu block, during the last glacial maximum (LGM; Fig. 1b). It was 20–30 m higher than the coastal plain and 50–60 m higher than the palaeo-incised Changjiang and Qiantang valleys during the LGM. The major post-glacial Changjiang sediments deposited in the paleo-incised valley and coastal plain on both northern and southern flank (Li et al., 2000). Previous study demonstrated different sediment provenances during the Holocene, i.e., more local source from the western highland for the lacustrine plain and more Changjiang source for the coastal plain (Wang et al., 2006). Previous studies also suggested that the present dish-like morphology was formed as a result of post-glacial sea level rise and the development of chenier ridges around the margin of the Taihu block as the Changjiang delta built up and prograded eastwards (Stanley and Chen, 1996; Chen and Stanley, 1998; Wang et al., 2006).

Tectonic subsidence has occurred in this area since the Late Pliocene due to subduction of the Philippine oceanic plate, which caused the sinking of the Fukien–Reinan massif that extends across the East China Sea continental shelf to the Korean peninsula (Wageman et al., 1970; Chen and Stanley, 1995). Several series of NW–SE and NE–SW faults, and small NE-SW anticlines and synclines occur in the study area (Fig. 1c). The paleotopography of the Late Cenozoic basement was characterized by highlands in the western and south-western

areas and NE-oriented valleys in the northeast. Fluvial and lacustrine sedimentation dominated during the early Pleistocene, while coastal and shallow marine deposits have appeared mainly since the mid-Pleistocene (Lin et al., 1989; Chen et al., 1997). The Changjiang River originally occupied a more northerly position and has moved to its current location only during the Holocene (Chen and Stanley, 1995; Xiao et al., 2004).

3. Methods

We obtained a 105 m deep borehole, QP88 in 2007 and a 51.2 m deep borehole, WJ in 2008 from the Taihu block of southern Changjiang delta plain (Fig. 1). Both boreholes were drilled using a rotary rig with a corer diameter of 9.2 cm. Fine-grained sediments dominate the mid-Pleistocene to Holocene strata in both boreholes.

OSL dating samples were immediately taken when the boreholes were drilled. Three samples of clayey silt and fine sand were taken from WJ and five samples of silt and fine sand from QP88. The samples from WJ were measured using a Risø-TL/OSL-DA-20 reader with an attached EMI 9235QB15 photomultiplier tube and a $^{90}Sr/^{90}Y$ beta source in School of Earth and Environmental Sciences, University of Wollongong, Australia (Table 1). Samples from QP88 were measured using a Risø-TL/OSL-15 reader with a $^{90}Sr/^{90}Y$ beta source at the Laboratory for Earth Surface Processes, Peking University (Table 2). After trimming off the outer rim of each sample, about 300 g were taken for preparation for the aliquots of quartz fractions (4–11 μm): Hydrogen Peroxide (H_2O_2) and HCl were used to remove the organic matter and carbonate before the component of 4–11μm was settled; Fluosilicic acid (40%) was used to remove the feldspar from the settled fraction. Single-aliquot regeneration (SAR)

procedure was used to determine the equivalent dose of each aliquot. Twenty (20) to 30 aliquots were tested for each sample and only aliquots with low recuperation (<5% of the natural signal) and low IR depletion ratio (<10%) were selected. Central Age Model (CAM) was used to obtain the final equivalent doses for each sample. The Minimum Age Model (MAM) was also used for sample UOW-313 from WJ (Table 1) since the distribution of equivalent doses of all selected aliquots has a greater spread on the radial plot (Fig. 2). Besides, about 20 g sediments were taken for measuring the moisture content and concentrations of U, Th, and K. U and Th was derived from thick-source alpha counting and K was derived from XRF. Gamma dose rates were calculated from concentrations of U, Th, and K. Cosmic dose rates were estimated using the geomagnetic longitude/latitude, altitude and burial depth of the sample (Prescott and Hutton, 1994).

To validate the OSL ages of two boreholes, AMS^{14}C and paleomagnetic dating was further applied for WJ and U-series dating for QP88. Two shell samples were selected from WJ for AMS^{14}C dating at Beta Analytic (Table 3). We calibrated the conventional radiocarbon ages into calendar ages using the calibration curve CalPal_2007_HULU by Weninger and Jöris (2008) and ΔR value 135±42 (Yoneda *et al*., 2007) is used to remove the marine reservoir effect. U-series analysis was carried out on three shell samples of *Potamocorbula amurensis* (estuarine water species) and *Corbicula leana* (freshwater to brackish water species) from QP88 (Table 4). Sample preparation and measurements were done at the Institute of Geology and Geophysics, Chinese Academy of Sciences. An Octête® PLUS 8-unit Alpha Spectrometer and the ISOPLOT/EX program was employed to determine the age using the method described in Ma et al. (2004).

Ninety-nine samples from WJ were taken for measurement of magnetic susceptibility with a dual-frequency (0.47 and 4.7 kHz) sensor from Bartington Instruments (noise level ~10^{-9} m^3 kg^{-1}). Paleomagnetism was further measured on 376 samples from WJ in a magnetic field free space (<150nT) at the Institute of Earth Environment, Chinese Academy of Sciences. Progressive thermal demagnetization was carried out firstly by heating samples to 620°C at an interval of 10-50°C with an ASC Scientific TD-48 instrument, followed by the remanence measurement with a 2G755 superconducting magnetometer. The orthogonal projections of progressive thermal demagnetization revealed that secondary viscous remanent magnetization (VRM) of most samples were removed at a low temperature generally below 200-300°C (Fig. 3). The direction of remanent magnetization (RM) above 300 °C then became relatively stable and trended to the origin of the orthogonal plot, representing the direction of primary characteristic RM. Meanwhile, NRM was the maximum at the room temperature, and the intensity reduced to <10% of NRM while temperature increased to 650 °C (Fig. 3). Therefore, at least four successive demagnetization components above 300 °C were used to calculate the direction of primary characteristic RM of each sample by principal component analysis.

Besides, sediment grain size analysis was carried out on 99 samples from WJ and 174 from QP88 by a Beckman Coulter Laser Diffraction Particle Size Analyzer (LS13320). Twenty-two samples from WJ and 82 from QP88 were taken for foraminiferal analysis. Eighty samples from QP88 above core depths of 55 m were taken for pollen-spore analysis. Freshwater and marine algae were also identified when analysing the pollen-spore samples from QP88 sediments. Fossil gastropods and bivalves from QP88 were identified in the Nanjing Institute of Geology and Palaeontology, Chinese Academy of Sciences (Tables 5–6).

We also compiled our previously published borehole data, SG7 (Wang et al., 2008), FX and MFC (Zhao et al., 2008), including lithology and stratigraphy, OSL and U-series dates, fossil foraminifera and pollen-spore, and re-interpreted the sedimentary environment and chronostratigraphy. We compared the strata of these boreholes, which were obtained from the coastal plain of the southern Changjiang delta plain, with those of WJ and QP88 from the Taihu block.

4. Results

4.1. Stratigraphy and distributions of foraminifera and pollen-spore

4.1.1. Holocene

The Holocene sediment (S1) in WJ (core depth 0–2.5 m) and QP88 (core depth 0–3.3 m) is characterized by clayey silt and silty clay that is brownish yellow in the upper part and dark grey in the lower part (Figs 4–5). Root traces and Fe/Mn oxides are present in the upper half. A thin layer of peat occurs at the bottom in QP88. No foraminiferal fossils were found (Fig. 6) but the pollen-spore spectrum is extremely rich, characterized by the dominance of *Quercus*–*Pinus*–Gramineae–*Typha*–Cyperaceae (Fig. 7). Magnetic susceptibility of the Holocene sediment in WJ is low, being around 10×10^{-9} m^3 kg^{-1} (Fig. 4). The Holocene sediment in SG7 (core depth 0–24.3 m) is composed of grey and dark grey silty clay interbedded with thin layers of silt in the middle and lower sections, grey silt in the upper, and yellowish grey and grey clayey silt on the top (Fig. 8). Two OSL ages are 3.8±0.3 ka at 8.3 m and 15.0±1.4 ka at 24 m. Rich foraminiferal and pollen-spore assemblages are present, including common *Castanea* and *Quercus* pollen that is typical of warm and humid

environments and *Typha* that represents a wetland flora (Fig. 8).

4.1.2. Late Pleistocene

Five sedimentary units were recognized within the late Pleistocene depositional succession in the boreholes.

S2-1: A layer of yellowish grey, brownish yellow or dark green stiff mud occurs on the top of late Pleistocene sedimentary succession at 2.5–5.7 m in WJ, 3.3–6.3 m in QP88 and 24.3–27.1 m in SG7 (Figs 4–5, 8). This stiff mud is formed by pedogenesis during the LGM (Li et al., 2000; Chen et al., 2008), supported by the OSL age 18.2±1.6 ka at 25 m in SG7. No marine microfossils were found in this palaeosol. Pollen-spore abundance is very low and *Concentricystes* is dominant (Fig. 7). Magnetic susceptibility is still as low as around 10×10^{-9} m^3 kg^{-1} in WJ (Fig. 4).

S2-2: Greyish yellow silt and silty sand with abundant Fe/Mn oxides underlies the paleosol at 6.3–8.0 m in QP88 and 27.1–43.4 m in SG7 (Figs 5, 8). It is not present in WJ (Fig. 4), then increases its thickness eastward from 1.7 m in QP88 to 16.3 m in SG7 (Fig. 9). Foraminifera and pollen-spores were only sporadically found. *Pinus*, *Betula*, *Quercus*, *Artemisia*, Gramineae are the main pollen (Figs 7–8). There is one OSL age 67±9 ka at 7.8 m in QP88 and one OSL age 59.3±3.5 ka at 40.5 m in SG7, both showing overage compared with the ages of underlying sediments (Table 2; Figs 5, 8).

S3: A 9 m thick fining-upward unit occurs at 5.7–14.5 m in WJ (Fig. 4), i.e., grey sand and silty clay interbedded thinly or thickly in the lower section, brownish and yellowish grey clayey silt with some silty clay in the middle section, and brownish clayey silt and silty clay

on the top. Burrows present at 7.8–10.8 m. Magnetic susceptibility increases obviously, especially below 11 m where it is around 35×10^{-9} m^3 kg^{-1} (Fig. 4). At 11.4 m, an OSL age is interpreted as 68±6 ka by CAM while it is 48±6 ka by MAM (Table 1). Radiocarbon dating show ages 42970±720 cal yr BP at 11.75 m and 44480±1270 cal yr BP at 14.2 m (Table 3). Paleomagnetism measurement indicates the Laschamp excursion (39–41 ka; Channell, 2006; Cassata et al., 2008) at core depth 11.2–11.9 m and possibly the Monolake excursion (*c.* 32 ka; Channell, 2006; Cassata et al., 2008) at around 8.3 m (Fig. 4). In QP88 and SG7 this unit is yellowish grey, grey and dark grey silty sand and silt at 8.0–22 m and 43.4–62.5 m (Figs 5, 8). Shell fragments occur in a few thin layers in SG7. OSL dating show two ages 27±3 ka at 10.05 m and 43±5 ka at 11.4 m in QP88 (Table 2). One U-series age 45.3±3.7 ka is obtained at 52.7 m is SG7 (Table 4).

Foraminiferal abundance fluctuates obviously in all three boreholes. We demonstrate its distribution in QP88 as an example here (Fig. 6). Foraminifera are present at core depth 8.0–12 m, dominated by *Elphidium magellanicum* and *Ammonia beccarii* var. The abundance increases remarkably at 12–16.5 m, and species of open water also appear as *Ammonia compressiuscula*, *Quinqueloculina*, *Bolivina cochei*, *Hanzawaia nipponinica* in addition to the typical coastal *Elphidiella kiangsuensis*. Abundance then declines at 16.5–22 m, predominated by the typical intertidal flat specie *Nonion akitaense* Asano (Fig. 6). The pollen-spore abundance is still low, except for a peak at the top of unit in both QP88 and SG7. *Quercus*, *Pinus* and *Carpinus* are the dominant tree species (Fig. 7). The warm and humid favoured species, like *Castanea* and *Castanopsis*, are also present. *Typha* and *Pteris* are the major herbaceous and fern species. Marine algae, mainly *Spiniferites* spp. appear in the lower

and top sections of this unit.

S5-1: This marine-influenced unit of S5-1 is mainly composed of fine-grained sediments (Figs 4–5, 8). In WJ couplets of silt and silty clay dominate at core depth 14.5–27.4 m. Thickness of the silt laminae is generally less than 0.5 cm but reaches *c.* 2 cm at the top and bottom. Burrows occur at 17–20 m. OSL dating shows an age 73±6 ka at 22.7 m (Table 1). Paleomagnetism measurement reflect possible the Norwegian-Greenland Sea event (*c.* 64.5 ka; Arz et al., 2007) at core depth 16–17 m (Fig. 4). Magnetic susceptibility remains high at around 35×10^{-9} m^3 kg^{-1} (Fig. 4). In QP88 dark grey, grey and greenish grey clayey silt occurs along with fine sand and two layers of mollusc shells at core depth 22–34.1 m and dark greenish grey stiff mud at 34.1–37 m. The shells are mainly intertidal gastropods, including *Umbonium* sp., *Umbonium thomasi* (Crosse), *Nassarius (Phrontis) caelatulus, Assiminea cf. colombeliana,* and *Cerithidea* sp., and the shallow marine species of *Mitrella* sp. (Table 5). Fresh to brackish water and estuarine bivalves are also present and include *Corbicula leana*, *Corbicula largillerti*, *Ostrea* sp., *Silqua mimima* and *Potamocorbula amurensis* (Table 6). There are three OSL ages, 61±6 ka at 22.25 m, 77±7 ka at 22.9 m and 78±9 ka at 28.3 m (Table 2) and two U-series ages 68.2±4.7 ka at 22 m and 79.1±3.2 ka at 29.2 m (Table 3). In SG7 the lithology comprises dark grey, grey and bluish grey silty clay with thin layers of silt at core depth 62–74 m. Mollusc shells are also abundant at core depth 65.75 m and 72.4 m and species are mainly *Corbicula* and *Potamocorbula amurensis*. Two OSL ages are 69.0±5.1 ka at 62 m and 74.2±2.5 ka at 62 m (Table 2) and two U-series ages are 63.0±3.6 ka at 65.75 m and 85.9±6.1 ka at 72.4 m (Table 4).

Foraminifera are rare to abundant in WJ and QP88, while they are sporadic in SG7. High

abundance occurs at 22–29.5 m in QP88 and dominated by coastal species *Ammonia beccarri* var., *Elphidium magellanicum*, *Nonion*, *Cribrononion* (Fig. 6). There appears both typical tidal flat species including *Elphidiella kiangsuensis*, *Pseudononionella variabilis* and *Nonion akitaense* Asano and open water species *Florilus*, *Quinqueloculina* and *Hanzawaia nippoinica*. The abundance reduces to rare to none at 29.5–37 m, mainly *Ammonia beccarri* var., *Elphidium magellanicum*, *Elphidiella kiangsuensis* and *Cribrononion* Thalmann (Fig. 6). Marine algae also present in QP88, mainly *Spiniferites* spp. (Fig. 7). Abundance of pollen and spores is low but increases remarkably in the middle section in both QP88 and SG7. The assemblage is characterised by high percentages of *Quercus* (deciduous), *Pinus*, *Ulmus*, *Carpinus* and *Betula* that suggest a moist temperate climate (Figs 7–8).

S5-2: In WJ S5-2 is a coarsening-upward unit of dark grey fine sand with mud laminations in the lower section at 27.4–34.3 m (Fig. 4). Magnetic susceptibility reaches its highest value of 93×10^{-9} m^3 kg^{-1} at the top of this unit and decreases downwards to 27×10^{-9} m^3 kg^{-1}–55×10^{-9} m^3 kg^{-1}. The paleomagnetic Blake event (114–120 ka; Zhu et al., 1994; Fang et al., 1997) was recorded at core depth 27.4–30.0 m. Meanwhile, an OSL age 100±8 ka was obtain at 28.3 m. At 37–52 m of QP88 sediment consists mainly of grey and greenish grey silty clay and is interbedded with clayey silt in the lower section. There are some gastropod and mollusc shells of fresh to brackish water species including *Bellamya* sp., *Corbicula leana* and *Corbicula largillerti* at core depth 48–50 m (Tables 5–6). In SG7 the lithology comprises grey to brownish grey clayey silt and silt with some laminations of fine sand at 74–86.5 m.

Foraminifera are abundant in the middle section and present in both bottom and upper sections in WJ and they are abundant in upper section and present in lower section in QP88.

There is none in SG7. Dominant species are coastal and tidal flat ones including *Ammonia beccarri* var., *Elphidium magellanicum, Elphidiella kiangsuensis, Pseudononionella variabilis* and *Nonion akitaense*. There are also some open water species of *Florilus, Ammonia compressiuscula* and *Bolivina cochei* (Fig. 6). Pollen and spores are generally plentiful but fluctuate in abundance. There are *Quercus* (evergreen), *Castanea*, *Castanopsis* and *Ilex* which are typical of a warm and humid environment, while the percentages of temperate species *Betula* and *Ulmus* declined obviously to <5% and <10% (Figs 7–8). However, relative percentage of *castanea+castanopsis* decreases while *Abies+Picea* increase. Of note, the salt-tolerant Chenopodiaceae increases upward significantly in S5-2 of QP88 (Fig. 7). Besides, a rich marine algae flora is present in QP88, mainly the warm water *Spiniferites* spp. which were found continuously (Fig. 7).

4.1.3. Mid-Pleistocene

The top of the mid-Pleistocene succession in WJ and QP88 boreholes is represented by a stiff mud unit (Figs 4–5). Very few pollen or spores were detected in this top muddy sediment (Fig. 5). In WJ it is *c.* 5 m thick and is underlain by a succession of homogeneous silty clay with silt laminations, stiff mud with organic matter, and homogeneous silt (Fig. 4). Magnetic susceptibility shows low-high-low cycles. In QP88 it is underlain by a succession of silty clay and silt or silty sand units that may represent three cycles of deposition (Fig. 5). Foraminifera are present in the upper but absent in the lower section in WJ, and are absent or rare in most sections but are abundant locally in an upper succession in QP88. Species are predominantly coastal and tidal flat ones (Fig. 6). The mid-Pleistocene sediment recovered from SG7 is

generally coarse-grained (i.e., sand and gravely sand) on the top, underlain by bluish grey clayey silt with shell fragments. No marine microfossils were found. Pollen and spores are rare in the sandy section but rich in the mud (Fig. 8).

5. Discussion

5.1. Interpretation of sedimentary facies and chrono-stratigraphy of the late Pleistocene

Intertidal to subtidal facies were interpreted for the unit S5-2 in three boreholes from the species of gastropod and mollusc shells, foraminifera, marine ages and the abundant occurrence of Chenopodiaceae (Tables 5–6; Figs 5–7). The highest values of magnetic susceptibility in WJ also indicate features of coastal sediments (Fig. 4; Kwon et al., 2011). Ages from different dating methods reflect unit S5-2 are deposited during the period of *c.* 134–100 ka. We suggest that this unit can be equated with the OIS 5e and possibly 5c of sea level highstand. This could also be deduced from the warm and humid climate reflected by pollen-spores (Figs 7–8) and the strongest marine invasion reflected by the highest abundance of foraminifera in WJ (Fig. 4), continuous occurrence of high percentage of marine algae and the most abundant pollen of salt-tolerant Chenopodiaceae in QP88 (Fig. 7). Freshwater influx should be also the greatest due to the warm and humid climate because fresh to brackish water species of gastropod and mollusc dominate the shells in QP88 (Tables 5–6). This could explain the relative low percentages of open water species of foraminifera (Wang, 1980) and low percentage of local tree pollen *castanea+castanopsis* versus increased percentage of *Abies+Picea*. The trees of *Abies* and *Picea* don't grow in the study area and pollens were possibly transported from upper Yangtze by the runoff of Changjiang River (Chen et al.,

2009). The lack of foraminifera in S5-2 in SG7 could be caused by the influx of freshwater and sediment discharge or dissolution during the early diagenesis due to the warm and humid climate (Wang, 1980).

High values of magnetic susceptibility and the presence of foraminifera in the overlying S5-1 unit of WJ indicate a tidal flat environment (Kwon et al., 2011). The foraminifera species and the occurrence of both shallow marine and intertidal gastropod and both estuarine and fresh to brackish water bivalves in QP88 indicates sedimentary environment changing from intertidal flat to estuary and then to intertidal flat again from bottom upward (Figs 5–6; Tables 5–6). Ages range mainly from *c.* 86 ka to 61 ka (Figs 4–5, 8) and would represent deposition in OIS 5a. The stiff mud in bottom section in QP88 probably represents dewatering during a period of exposure during OIS 5b. There is no stiff mud in WJ and SG7 and erosion could have occurred during OIS 5b since an abrupt lithology change happens between S5-2 and S5-1. In the earlier boreholes (FX and MFC) S5 consists mainly of sandy and gravely sandy successions of fluvial channel formation and has ages from *c.* 66 ka to *c.* 113 ka (Fig. 9), indicating a paleo-incised valley prevailed at these two core locations during the sea level lowstands of OIS4, 5b and 5d. They are probably equivalent to fluvial successions in borehole JD1 that were interpreted by Chen and Stanley (1995) to have been derived from the Tian-mu-shan highlands west of Taihu Lake (Fig. 1c), rather than from the Changjiang River.

The occurrence of foraminifera from present to abundant and the abrupt decrease in magnetic susceptibility in S3 in WJ possibly indicates sedimentary environment changing from intertidal to subtidal flat. The fluctuations in foraminifera abundance and species suggest a cycle of sedimentary environment from intertidal to subtidal and then to intertidal again

from bottom upward in S3 of QP88 (Figs 5–6). By contrast, the sedimentary features, i.e. the shelly silt and silty sand with Fe and Mn oxides and relative high abundance of foraminifera in S3 of SG7 may suggest an environment of low energy beach (Fig. 8).

We suggest that the OSL age 48±6 ka resulted from MAM is more reliable at core depth 11.4 m in WJ because it fits better with not only the AMS ^{14}C ages and paleomagnetic event, but also the sedimentation rates of different time periods in WJ (Table 1; Fig. 4). We suggest the incomplete bleaching of sediment associated with rapid deposition resulted in the older age of 68±6 ka. S3 can also be correlated with equivalent marine sections in MFC and FX that provided ages ranging from *c.* 50–32 ka BP (Fig. 9; Zhao et al., 2008). Therefore, we suggest an age spanning from *c.* 50 to *c.* 27 ka BP is reasonable for S3 which mainly would have been deposited during the later transgressive phase of OIS 3.

The sedimentary features of abundant Fe and Mn oxides and lack of foraminifera indicate an oxidized environment and sheetwash facies is explained for unit S2-2 (Figs 5, 8). Ages of S2 range from *c.* 23 ka to10 ka, based on OSL dating from FX and MFC (Fig. 9; Zhao et al., 2008). Two anomalous OSL ages of *c.* 67 ka and 59 ka were obtained from S2-2 in QP88 and SG7, respectively (Figs 5, 8). We suggest that these ages come from a non-marine deposit probably formed at the start of the OIS 2 regression and may represent poorly bleached muddy mass-flow deposits derived from an adjacent older (OIS 3 or even OIS 5) exposed succession before adequate vegetation had become established.

5.2. Estimation of OIS 3 relative sea level

The relative sea level can be estimated as the burial depth of marine-influenced strata

minus the palaeo-water depth and extent of subsidence caused by sediment compaction and tectonic movement. The lithology and marine fauna in the unit S3 in WJ, QP88 and SG7 indicate intertidal to subtidal flat or low energy beach environments that formed near the mean sea level (Figs 4–5, 8). Intertidal to subtidal environment is also suggested for unit S5-2. Hence the palaeo-water depth of intertidal to subtidal sediments in both S3 and S5-2 is around 2–-5 m (Yellow Sea datum). Suppose the highstand of sea level during OIS 5e is 5 m above the PMSL (Chappell et al., 1996), then elevation of subtidal facies should be around PMSL and elevation of intertidal facies is 7–2 m above PMSL. A mean rate of subsidence since OIS 5e can be calculated by dividing the burial depth of OIS 5e by its age after the palaeo-water depth is removed. Then a mean subsidence rate of *c*. 0.25 m/ka for WJ, *c*. 0.34 m/ka for QP88, and *c*. 0.69 m/ka for SG7 can be derived by dividing the burial depth of subtidal flat sediments formed during OIS 5e by their absolute ages. Therefore, the relative sea level for S3 was *c*. -2.5 m to 1.2 m at core location WJ, -4.0 m to 1.2 m at QP88, and -27.5 m to -24.8 m at SG7 assuming the base of S3 to be 50 ka and top at 27 ka.

5.3. Comparison of OIS 3 sea level records with other areas in the world

Sea level histories have been determined from oxygen isotope studies of deep sea core sediments (Chappell et al., 1996; Linsley, 1996; Siddall et al., 2003), which suggested that maximum sea level during the early stage of OIS 3 could have been as high as -20 m to -30 m, then sea level dropped to -50–-65 m during the latter part of OIS 3. The main advantage of the deep sea sediments is that they provide a continuous record of sedimentation not punctuated by the uncertainties in shallow water records caused by exposure and erosion during

regressions. The records from deep sea benthic foraminifera show a similar pattern of deep sea water temperature changes that match the sea level fluctuations (Waelbroeck et al., 2002). Raised coral terraces provide useful sea level indicators to compare with the deep sea records. Dated coral reef sequences of OIS 3 age have been described from the Huon Peninsula (Papua New Guinea, Chappell et al., 1996) and Malakula (Vanuatu, Cabioch and Ayliffe, 2001). Both these successions show an early OIS 3 highstand at -30–-56 m during 45–52 ka, followed by a decrease in sea level to -50–-70 m during the latter part of OIS 3. Peltier and Fairbanks (2006) suggested that the sea level recorded at Barbados is 80–90 m below PMSL during the late OIS 3. The succession in the Gulf of Carpentaria in northern Australia represents another well preserved late Quaternary record of sea level fluctuations on a large relatively stable epicontinental shelf. Detailed analyses based on ostracod and coccolith assemblages preserved in OIS 3 strata from the central part of the gulf provide a detailed record of environmental change since the start of the last interglacial and estimated a sea level of -50 m during OIS 3 (Chivas et al., 2001; Couapel et al., 2007; Reeves et al., 2007, 2008).

In contrast to these lower OIS 3 sea level records, a very well documented record of OIS 3 sea level on a tectonically stable coastline in South Australia has been examined by Cann et al. (1988, 1993). This study recorded sea level fluctuations between -26 m and -37 m during the period from 45 ka to 32 ka based on foraminiferal data together with radiocarbon and amino acid racemisation (AAR) chronology. The equivalent OIS 5e sea level in this same region is at +2 m indicating that the area has not been uplifted since OIS 5 (Murray-Wallace, 2002).

A high relative sea level record of <30 m below PMSL for OIS 3 has also been reported

in other areas in the world during recent decade. For example, Hanebuth et al. (2006) found a sea level highstand of 16–26 m below PMSL during late OIS 3 age based on AMS radiocarbon dating in the Red River delta. They suggested that either it resulted from differential subsidence and partial uplifting or that all the radiocarbon dates were contaminated by younger material. Similar phenomenon can be found in other previous studies of Indochinese deltas. For example, an AMS ^{14}C date of 43.4 ka BP was obtained for undifferentiated shallow marine sediment buried at a depth of 25 m below PMSL in the Mekong delta, Vietnam (Ta et al., 2002). AMS^{14}C dates of 36.3–44.7 ka BP were also obtained from undifferentiated shallow marine sediment buried at a depth of *c.* 14 m below PMSL in the Chao Phraya delta, Thailand (Tanabe et al., 2003). In northeastern North Carolina, Parham et al. (2007) examined the sedimentary sequences in both drill-holes and seismic profiles and summarized all the available radiocarbon, AAR and OSL age determinations. They found elevations of OIS 3 highstand deposits that indicate sea level was either similar to the present or that the region has been influenced by glacio-isostatic adjustment. Mallinson et al. (2008) confirmed the age of OIS 3 coastal deposits by OSL analyses on quartz grains from palaeo-shoreline deposits and suggested either the glacio-isostatic adjustment was as large as 22–26 m or that the OIS 3 sea level was briefly higher. Wright et al. (2009) used ^{14}C and AAR ages and high-resolution seismic reflection profiles to derive a highstand OIS 3 sea level of 25 m below PMSL on the New Jersey margin.

5.4. Possible mechanisms for the high OIS 3 sea level record in the study area

Sediment compaction could firstly used to explain the difference in positions of OIS 5 marine-influenced sediments in cores QP88, WJ and SG7. We suggest that larger extend of sediment compaction occurred in core SG7 than in other two cores, since there is no stiff mud at the base of late Pleistocene strata in SG7. Stiff mud of the palaeosol is impermeable and generally serves as aquiclude for the ground water (McArthur et al., 2008). Thus pore water is easier to lose in SG7 during the periods of low sea level stand, causing stronger sediment compaction. Even with the subsidence effect caused by sediment compaction, the relative sea level records of late OIS 3 from WJ and QP88 are at least 25–30 m higher than the global sea level as synthesized above, while elevation of OIS 3 sediments in SG7 match with the position of palaeo-sea level. Therefore, we suggest that the Taihu block where cores WJ and QP88 locate should have been raised after the end of OIS 3. Reasons for the time of uplift include Holocene sediments of only <5 m thick happen without marine invasion over the Taihu Lake area, while OIS 5 and OIS 3 marine influenced sediments exist over the study area (Figs 1b, 9). Factors must be taken into consideration including glacio- hydro- isostacy adjustment and tectonic movement.

Potter and Lambeck (2003) provided a model based on glacio- hydro- isostacy to account for the apparent discrepancies between the OIS 5e and OIS 5a sea-level data for the western North Atlantic Ocean area. They showed that the slower response time for isostatic versus ice volume changes has left a bulge with over 30 m positive relief over a distance of about 4300 km between the position of the ice sheet and Barbados. This accounts for the apparently high OIS 3 sea level observations in Bermuda (e.g. Bard et al., 1990), North Carolina (e.g. Parham et al., 2007; Mallinson et al., 2008) and New Jersey (Wright et al., 2009).

A similar approach was considered for assessing the high OIS 3 sea level determined for the Changjiang delta and the other major Indochinese deltas as documented by Ta et al. (2002), Tanabe et al. (2003), and Hanebuth et al. (2006). In this region sites on the exposed continental margin show OIS 3 sea level at maximum elevations of -5 m to -25 m whereas on the outer parts of the equivalent continental shelves sea level indicators are at depths of -50 m to -70 m. The position of northern ice sheets in the Siberian region has been the subject of discussion in the literature with Gosswald (1998) and Grosswald and Hughes (2002) suggesting extensive LGM ice sheets in Arctic and Pacific Siberia with considerable ice volumes. Such ice sheets could possibly have caused uplift in Southeast Asia although they are probably still located too far from the uplift sites. However, later research in eastern Siberia (Beringia) has shown that most of the large ice advances reflect earlier glacial events and that ice was relatively minor in the LGM (e.g, Sher, 1995; Brigham-Grette, 2001; Brigham-Grette et al., 2001, 2003; Glushkova, 2001; Heiser and Roush, 2001; Siegert et al., 2001; Gualtirei et al., 2003). The lack of an East Siberian ice sheet is also favoured by vegetation modelling (Felzer, 2001). Thus a glacio-hydro-isostatic bulge caused by a northern ice sheet cannot be contemplated as a plausible mechanism for the high OIS 3 sea level records in the Asian megadelta areas.

The most plausible explanation for the raised OIS 3 deposits adjacent to the Asian megadeltas (Changjiang, Red River, Mekong and Chao Phraya) is isostatic loading and differential subsidence caused by the deposition of significant volumes of sediment in the deltas and adjacent offshore areas on the wide continental shelves surrounding these areas in the East China Sea and Sunda Shelf as suggested by Hanebuth et al. (2006). In the case of the

study area the region near Taihu Lake may be influenced by the combined sediment accumulation of both the Changjiang and Huanghe Rivers. The postglacial sediment load deposited annually by the Changjiang River is estimated to be 236–486 Mt (Li et al., 2003). The thickness of Quaternary, including Holocene, sediments to the north of the study area is over 400 m with the load progressively shifting southeastward with time as the Changjiang River shifted its position (Fig. 1c; Chen and Stanley, 1995). The current main depositional lobes of the Changjiang delta extend for over 50 km seaward from the mouth of the estuary (Chen et al., 2000). There is also a huge delta lobe of the abandoned Yellow River along the adjacent coast of Yellow Sea (Ren and Shi, 1986). Therefore, sediment load on the continental shelf of eastern China marginal sea would have caused differential subsidence of the study area and adjacent continental shelf.

In addition, tectonic subsidence prevailed in the study area due to the sinking of the Fukien-Reinan massif to the east of the Changjiang coast since the Late Pliocene (Wageman et al., 1970). The position of the OIS 5e sediments in all boreholes may provide the evidence. However, southeastward shifting of the Changjiang River mouth during the Quaternary, especially the deposition of thick postglacial sediments in the southern Yellow Sea and on the Changjiang coast have lead to northeastward tilting of the Changjiang coast. Therefore subsidence of the Taihu block ceased and was replaced by uplift. Further, due to the existence of NW-SE extentional faults in the study area (Fig. 1c), tilting transferred to the Taihu block may be not gentle but may have been amplified significantly.

Tilting in this region may control the extent of the Holocene transgression and the location of the Holocene highstand chenier ridges (Fig. 1a). In fact, such isostatically-induced

tilting and uplift may still be occurring in the Changjiang delta region. In the modern Changjiang delta the 4 ka junction between the subtidal to lower intertidal flats and the upper intertidal flats now occurs at approximately +5 m some 200 km inland from the present delta mouth at HQ98 (Fig. 8 in Hori et al., 2002). This could reflect a fall of relative sea level since 4 ka (Hori et al., 2001) combined with load-induced tilting and hinterland uplift caused by rapid increase in sediment load as the Changjiang delta prograded.

6. Conclusions

Dating and stratigraphic analysis have demonstrated that a succession of OIS 3 deposits over 10 m thick extended across the southern Changjiang delta plain. This OIS 3 sequence overlies OIS 5 deposits and has a greater vertical range than the OIS 5 deposits.

The OIS 3 deposits represent tidal flat and low energy beach sequences from west to east in the study area. Intertidal to subtidal deposits of OIS 5e also occur and the position of these latter units in the boreholes indicates at least 30–80 m of subsidence since OIS 5e.

The present distribution of OIS 3 strata means that either the late OIS 3 sea level was equivalent to present sea level (unlikely) or the Taihu Lake area must have undergone subsidence to at least -30 m to accumulate the deposits of OIS 5 and 3, followed by 25–30 m of uplift to bring them to their present position.

The initial subsidence phase was probably related to the regional subsidence of the Fukien-Reinan massif. The subsequent uplift is associated with north-northeast tilting of the Taihu block as a result of isostatic downwarping caused by the rapid growth of the Changjiang and abandoned Huanghe deltas.

Acknowledgements

The study was supported for design and research by the National Natural Science Foundation of China (Grant no. 41176070) and the grant from the Ministry of Science and Technology of China (Grant No. SKLEC-2010RCDW05). Thanks are also given for writing and submission for publication to the Chinese “111” Programme (Grant no. B08022)

References

Arz, H.W., Lamy, F., Ganopolski, A., Nowaczyk, N., Pätzold, J., 2007. Dominant Northern Hemisphere climate control over millennial-scale glacial sea-level variability. Quaternary Science Reviews 26, 312–321.

Bard, E., Hamelin, B., Fairbanks, R.G., 1990. U-Th ages obtained by mass spectrometry in corals from Barbados: sea level during the past 130,000 years. Nature 346, 456–458.

Brigham-Grette, J., 2001. New perspectives on Beringian Quaternary paleogeography, stratigraphy, and glacial history. Quaternary Science Reviews 20, 15–24.

Brigham-Grette, J., Hopkins, D.M., Ivanov, V.F., Basilyan, A.E., Benson, S.L., Heiser, P.A., Pushkar, V.S., 2001. Last Interglacial (isotope stage 5) glacial and sea-level history of coastal Chukotka Peninsula and St. Lawrence Island, Western Beringia. Quaternary Science Reviews 20, 419–436.

Brigham-Grette, J., Gualtiere, L.M., Glushkova, O.Y., Hamilton, T.D., Mostoller, D., Kotov, A., 2003. Chlorine-36 and ^{14}C chronology support a limited last glacial maximum across central Chukotka, northeastern Siberia, and no Beringian ice sheet. Quaternary Research

59, 386–398.

Cabioch, G., Ayliffe, L.K., 2001. Raised coral terraces at Malakula, Vanuatu, southwest Pacific, indicate high sea level during marine isotope stage 3. Quaternary Research 56, 357–365.

Cann, J.H., Belperio, A.P., Gostin, V.A., Murray-Wallace, C.V., 1988. Sea level history, 30,000 to 45,000 yr BP, inferred from benthic foraminifera, Gulf St Vincent, South Australia. Quaternary Research 29, 153–175.

Cann, J.H., Belperio, A.P., Gostin, V.A., Rice, R.L., 1993. Contemporary benthic foraminifera in Gulf St Vincent, South Australia, and a refined Late Pleistocene sea-level history. Australian Journal of Earth Sciences 40, 197–211.

Cassata, W.S., Singer, B.S., Cassidy, J., 2008. Laschamp and Mono Lake geomagnetic excursions recorded in New Zealand. Earth and Planetary Science Letters 268, 76–88.

Channell, J.E.T., 2006. Late Brunhes polarity excursions (Mono Lake, Laschamp, Iceland Basin and Pringle Falls) recorded at ODP Site 919 (Irminger Basin). Earth and Planetary Science Letters 244, 378–393.

Chappell, J., 2002. Sea level changes forced ice breakouts in the Last Glacial cycle: new results from coral terraces. Quaternary Science Reviews 21, 1229–1240.

Chappell, J., Shackleton, N.J., 1986. Oxygen isotopes and sea-level. Nature 324, 137–140.

Chappell, J., Omura, A., Esat, T., McCulloch, M., Pandolfi, J., Ota, Y., Pillans, B., 1996. Reconciliation of late Quaternary sea levels derived from coral terraces at Huon Peninsula with deep sea oxygen isotope records. Earth and Planetary Science Letters 141, 227–236.

Chen, J., Wang, Z., Li, X., Chen, Z., 2009. Provenance of *Picea* and *Abies* pollens in late Quaternary sediments of the Yangtze River delta. Quaternary Sciences 29, 290–298 (in Chinese, with English abstract).

Chen, Q., Li, C., Li, P., Liu, B., Sun, H., 2008. Late Quaternary palaeosols in the Yangtze delta, China, and their palaeoenvironmental implications. Geomorphology 100, 465–483.

Chen, Z., Stanley, D.J., 1995. Quaternary subsidence and river channel migration in the Yangtze delta plain, eastern China. Journal of Coastal Research 11, 927–945.

Chen, Z.Y., Stanley, D.J., 1998. Sea-level rise on eastern China's Yangtze delta. Journal of Coastal Research 14, 360–366.

Chen, Z., Chen, Z., Zhang, W., 1997. Quaternary stratigraphy and trace-element indices of the Yangtze delta, eastern China, with special reference to marine transgressions. Quaternary Research 47, 181–191.

Chen, Z., Song, B., Wang, Z., Cai, Y., 2000. Late Quaternary evolution of the subaqueous Yangtze delta, China: sedimentation, stratigraphy, palynology, and deformation. Marine Geology 162, 423–441.

Chivas, A.R., García, A., van der Kaars, S., Couapel, M.J.J., Holt, S., Reeves, J.M., Wheeler, D.J., Switzer, A.D., Murray-Wallace, C.V., Banerjee, D., Price, D.M., Wang, S.X., Pearson, G., Edgar, N.T., Beaufort, L., De Deckker, P., Lawson, E., Cecil, C.B., 2001. Sea-level and environmental changes since the last interglacial in the Gulf of Carpentaria, Australia: an overview. Quaternary International 83-85, 19–46.

Couapel, M.J.J., Beaufort, L., Jones, B.G., Chivas, A.R., 2007. Late Quaternary marginal

marine palaeoenvironments of northern Australia as inferred from cluster analysis of coccolith assemblages. Marine Micropaleontology 65, 213–231.

Fang, X.-M., Li, J.-J., Van der Voo, R., Niocaill, C.M., Dai, X.-R., Kemp, R.A., Derbyshire, E., Cao, J.-X., Wang, J.-M., Wang, G., 1997. A record of the Blake Event during the last interglacial paleosol in the western Loess Plateau of China. Earth and Planetary Science Letters 146, 73–82

Felzer, B., 2001. Climate impacts of an ice sheet in east Siberia during the Last Glacial Maximum. Quaternary Science Reviews 20, 437–447.

Galbraith, R.F., Roberts, R.G., Laslett, G.M., Yoshida, H., Olley, J.M., 1999. Optical dating of single and multiple grains of quartz from Jinmium rock shelter, northern Australia: part I, experimental design and statistical models. Archaeometry 41, 339–364.

Glushkova, G.Y., 2001. Geomorphological correlation of Late Pleistocene glacial complexes of western and eastern Beringia. Quaternary Science Reviews 20, 405–417.

Grosswald, M.G., 1998. Late-Weichselian ice sheets in Arctic and Pacific Siberia. Quaternary International 45-46, 3–18.

Grosswald, M.G., Hughes, T.J., 2002. The Russian component of an Arctic ice sheet during the Last Glacial Maximum. Quaternary Science Reviews 21, 121–146.

Hanebuth, T.J.J., Saito, Y., Tanabe, S. Vu, Q.L., Ngo, Q.T., 2006. Sea levels during late marine isotope stage 3 (or older?) reported from the Red River delta (northern Vietnam) and adjacent regions. Quaternary International 145–146, 119–134.

Heiser, P.A., Roush, J.J., 2001. Pleistocene glaciations in Chukotka, Russia: moraine mapping using satellite synthetic aperture radar (SAR) imagery. Quaternary Science Reviews 20,

393–404.

Hori, K., Saito, Y., Zhao, Q., Cheng, X., Wang, P., Sato, Y., Li, C., 2001. Sedimentary facies and Holocene progradation rates of the Changjiang (Yangtze) delta, China. Geomorphology 41, 233–248.

Hori, K., Saito, Y., Zhao, Q., Wang, P., 2002. Architecture and evolution of the tide-dominated Changjiang (Yangtze) River delta, China. Sedimentary Geology 146, 249–264.

Kwon, M., Yun, S., Doh, S., Son, B., 2011. Metal enrichment and magnetic properties of core sediments from the eastern Yellow Sea, East Asia: implications for paleo-depositional change during the late Pleistocene/Holocene transition. Quaternary International 230, 95–105.

Li, B., Li, C., Shen, H., 2003. A preliminary study on sediment flux in the Changjiang delta during the postglacial period. Science in China (series D) 46, 743–752.

Li, C., Chen, Q., Zhang, J., Yang, S., Fan, D., 2000. Stratigraphy and palaeoenvironmental changes in the Yangtze delta during the Late Quaternary. Journal of Asian Earth Sciences 18, 453–469.

Lin, J., Zhang, S., Qiu, J., Wu, B., Huang, H., Xi, J., Tang, B., Cai, Z., He, Y., 1989. Quaternary marine transgressions and paleoclimate in the Yangtze River delta region. Quaternary Research 32, 296–306.

Linsley, B.K., 1996. Oxygen-isotope record of sea level and climate variations in the Sulu Sea over the past 150,000 years. Nature 380, 234–238.

Liu, J., Saito, Y., Wang, H., Zhou, L., Yang, Z., 2009. Stratigraphic development during the Late Pleistocene and Holocene offshore of the Yellow River delta, Bohai Sea. Journal of

Asian Earth Sciences 36, 318–331.

Ma, Z., Wang, Z., Liu J., Yuan, B., Xiao, J., Zhang, G., 2004. U-series chronology of sediments associated with Late Quaternary fluctuations, Balikun Lake, northwestern China. Quaternary International 121, 89–98.

Mallinson, D., Burdette, K., Mahan, S., Brook, G., 2008. Optically stimulated luminescence age controls on late Pleistocene and Holocene coastal lithosomes, North Carolina, USA. Quaternary Research 69, 97–109.

McArthur, J.M., Ravenscroft, P., Banerjee, D.M., Milsom, J., Hudson-Edwards, K.A., Sengupta, S., Bristow, C., Sarkar, A., Tonkin, s., Purohit, R., 2008. How paleosols influence groundwater flow and arsenic pollution: A model from the Bengal Basin and its worldwide implication. Water Resources Research 44, w11411.

Murray-Wallace, C.V., 2002. Pleistocene coastal stratigraphy, sea-level highstands and neotectonism of the southern Australian passive continental margin – a review. Journal of Quaternary Science 17, 469–489.

Parham, P.R., Riggs, S.R., Culver, S.J., Mallinson, D.J., Wehmiller, J.F., 2007. Quaternary depositional patterns and sea-level fluctuations, northeastern North Carolina. Quaternary Research 67, 83–99.

Peltier, W.R., Fairbanks, R.G., 2006. Global glacial ice volume and Last Glacial Maximum duration from an extended Barbados sea level record. Quaternary Science Reviews 25, 3322–3337.

Potter, E.-K., Lambeck, K., 2003. Reconciliation of sea level observations in the western North Atlantic during the last glacial cycle. Earth and Planetary Science Letters 217,

171–181.

Prescott, J.R., Hutton, J.T., 1994. Cosmic ray contributions to dose rates for luminescence and ESR dating: large depths and long-term time variations. Radiation Measurements 23, 497–500.

Reeves, J.M., Chivas, A.R., Garcia, A., De Deckker, P., 2007. Palaeoenvironmental change in the Gulf of Carpentaria (Australia) since the last interglacial based on Ostracoda. Palaeogeography, Palaeoclimatology, Palaeoecology 246, 163–187.

Reeves, J.M., Chivas, A.R., García, A., Holt, S., Couapel, M.J.J., Jones, B.G., Cendón, D.I., Fink, D., 2008. The sedimentary record of palaeoenvironments and sea-level change in the Gulf of Carpentaria, Australia, through the last glacial cycle. Quaternary International 183, 3–22

Ren, M.-E., Shi, Y.-L., 1986. Sediment discharge of the Yellow River (China) and its effect on the sedimentation of the Bohai and the Yellow Sea. Continental Shelf Research 6, 785–810.

Shackleton, N.J., 1987. Oxygen isotopes, ice volume and sea level. Quaternary Science Reviews 6, 183–190.

Sher, A., 1995. Is there any real evidence for a huge ice sheet in East Siberia? Quaternary International 28, 39–40.

Siddall, M., Rohling, E.J., Almogi-Labin, A., Hemleben, Ch., Meischner, D., Schmelzer, I., Smeed, D.A., 2003. Sea-level fluctuations during the last glacial cycle. Nature 423, 853–858.

Siegert, M.J., Dowdeswell, J.A., Hald, M., Svendsen, J-I., 2001. Modelling the Eurasian Ice

Sheet through a full (Weichselian) glacial cycle. Global and Planetary Change 31, 367–385.

Stanley, D.J., Chen, Z.Y., 1996. Neolithic settlement distributions as a function of sea level-controlled topography in the Yangtze delta, China. Geology 24, 1083–1086.

Syvitski, J.P.M., Kettner, A.J., Overeem, I., Hutton, E.W.H., Hannon, M.T., Brakenridge, G.R., Day, J., Vörösmarty, C., Saito, Y. Giosan, L., Nicholls, R.J., 2009. Sinking deltas due to human activities. Nature Geoscience 2, 681–686.

Ta, T.K.O., Nguyen, V.L., Tateishi, M., Kobayashi, I., Tanabe, S., Saito, Y., 2002. Holocene delta evolution and sediment discharge of the Mekong River, southern Vietnam. Quaternary Science Reviews 21, 1807–1819.

Tanabe, S., Saito, Y., Sato, Y., Suzuki, Y., Sinsakul, S., Tiyapairach, S., Chaimanee, N., 2003. Stratigraphy and Holocene evolution of the mud-dominated Chao Phraya delta, Thailand. Quaternary Science Reviews 22, 789–907.

Waelbroeck, C., Labeyrie, L., Michel, E., Duplessy, J.C., McManus, J.F., Lambeck, K., Balbon, E., Labracherie, M., 2002. Sea-level and deep water temperature changes derived from benthic foraminifera isotopic records. Quaternary Science Reviews 21, 295–305.

Wageman, J.M., Hilde, T.W.C., Emery, K.O., 1970. Structural framework of East China Sea and Yellow Sea. American Association of Petroleum Geologists Bulletin 54, 1611–1643.

Wang, P., 1980. Collection of papers on marine micro-faunas. Ocean Press, Beijing, pp204 (in Chinese).

Wang, Z., Chen, Z., Tao, J., 2006. Clay mineral analysis of sediments in the Changjiang delta plain and its application to the Late Quaternary variations of sea level and sediment provenance. Journal of Coastal Research 22, 683–691.

Wang, Z., Zhao, B., Chen, J., Li, X., 2008. Chronostratigraphy and two transgressions during the Late Quaternary in Changjiang delta area. Journal of Palaeogeography 10, 99–110 (in Chinese, with English abstract).

Wang, Z., Zhuang, C., Saito, Y., Chen, J., Zhan, Q., Wang, X., 2012. Early mid-Holocene sea-level change and coastal environmental response on the southern Yangtze delta plain, China: implications for the rise of Neolithic culture. Quaternary Science Reviews 35, 51–62.

Weninger, B., Jöris, O., 2008. A ^{14}C age calibration curve for the last 60 ka: the Greenland-Hulu U/Th timescale and its impact on understanding the Middle to Upper Paleolithic transition in Western Eurasia. Journal of Human Evolution 55, 772–781.

Wright, J.D., Sheridan, R.E., Miller, K.G., Uptegrove, J., Cramer, B.S., Browning, J.V., 2009. Late Pleistocene sea level on the New Jersey margin: implications to eustasy and deep-sea temperature. Global and Planetary Change 66, 93–99.

Xiao, S., Li, A., Jiang, F., Li, T., Wan, S., Huang, P., 2004. The history of the Yangtze River entering the sea since the Last Glacial Maximum: a review and looking forward. Journal of Coastal Research 20, 599–604.

Yang, S.L., Milliman, J.D., Li, P., Xu, K., 2011. 50,000 dams later: Erosion of the Yangtze river and its delta. Global and Planetary Change 75: 14–20.

Yoneda, M., Uno, H., Shibata, Y., Suzuki, R., Kumamoto, Y., Yoshida, K., Sasaki, T., Suzuki, A., Kawahata, H., 2007. Radiocarbon marine reservoir ages in the western Pacific estimated by pre-bomb molluscan shells. Nuclear Instruments and Methods in Physics Research B 259, 432–437.

Zhang, Y., Xue, Y.-Q., Wu, J.-C.,Yu, J., Wei, Z.-X., Li, Q.-F., 2008. Land subsidence and earth fissures due to groundwater withdrawal in the southern Yangtse delta, China. Environmental Geology 55, 751–762.

Zhao, B., Wang, Z., Chen, J., Chen, Z., 2008. Marine sediment records and relative sea level change during late Pleistocene in the Changjiang delta area and adjacent continental shelf. Quaternary International 186, 164–172.

Zhu, R.X., Zhou, L.P., Laj, C., Mazaud, A., Ding, Z.L., 1994. The Blake geomagnetic polarity episode recorded in Chinese loess. Geophysical Research Letters 21, 697–700.

Table headings

Table 1 Conventional OSL ages for sediment core samples from WJ together with supporting dose rate and equivalent dose data.

Table 2 Conventional OSL ages for sediments from QP88 and SG7 together with supporting dose rate and equivalent dose data.

Table 3 AMS ^{14}C dates for sediments from WJ together with $\delta^{13}C$ data. Calibration curve CalPal_2007_HULU by Weninger and Jöris (2008) and ΔR value 135±42 (Yoneda *et al*., 2007) were used to calibrated the ages, shown as the 1σ with 68% probabilities.

Table 4 U-series ages for sediments from QP88 and SG7 together with isotope ratios of $^{234}U/^{238}U$, $^{230}Th/^{232}Th$ and $^{230}Th/^{234}U$.

Table 5 Gastropods in OIS 5 sediments from QP88

Table 6 Bivalves in OIS 5 sediments from QP88

Figure captions

Figure 1 1a) Geographic location of the boreholes and study area at the mouth of the Changjiang drainage basin. The dish-like morphology of the present southern Changjiang delta plain is also shown; 1b) Isopachs of the Holocene sediment, indicating the morphologic high of the Taihu block and the major paleo-incised Changjiang and Qiantang valleys (after Wang et al., 2012); 1c) Isopachs of Late Cenozoic sediment, showing the SW-NE valleys in the paleotopography and active faults during the Late Cenozoic (after Zhang et al., 2008). There are also several small anticlines and synclines in the northwestern part of the study area.

Figure 2 Radial plots detailing the distributions of equivalent doses of aliquots for representative samples. Central Age Model (CAM) was used to determine the final equivalent dose for all samples and Minimum Age Model (MAM) was also used for the sample at 11.4 m of borehole QP88.

Figure 3 Orthogonal projections of progressive thermal demagnetization (left) and normalized intensity decay plots (right) for representative samples of borehole WJ. Shaded/open circles in the left plots represent projections onto horizontal/vertical planes. Ordinate and abscissa in the right plots represent nomolized intensity of remanent magnetization and temperature, respectively.

Figure 4 Comprehensive profile of WJ, including paleomagnetism, AMS ^{14}C and OSL ages, lithology profile and description, sediment composition, abundance of foraminifera, magnetic susceptibility, interpretation of sedimentary facies, and the corresponding OIS.

Figure 5 Comprehensive profile of QP88, including OSL/U-series ages, lithology profile and description, sediment composition, abundance of foraminifera, pollen-spores and marine algae, pollen-spore assemblage, interpretation of sedimentary facies, and the corresponding OIS.

Figure 6 Foraminifera distribution in QP88 showing by percentage of each species relative to the total abundance. Sedimentary environment is referred from the foraminifera assemblage. The codes from S1 to S5-2 represent the time of deposition from OIS 1 to OIS 5 for the strata.

Figure 7 Vertical distributions of arboreal and herbaceous pollen, ferny spore and marine

algae in QP88. The percentages of arboreal pollen are calculated from all the arboreal and terrestrial herbaceous pollen except the Gramineae, Cyperaceae, and Chenopodiaceae. The percentages of herbaceous pollen, ferny spore and marine algae are calculated from the total number of pollen, spore and algae. The codes from S1 to S5-2 represent the time of deposition from OIS 1 to OIS 5 for the strata.

Figure 8 Comprehensive profile of SG7, including OSL/U-series ages, lithology profile and description, sediment composition, abundance of foraminifera and pollen-spores, pollen-spore assemblage, interpretation of sedimentary facies, and the corresponding OIS (revised from Wang et al., 2008).

Figure 9 Stratigraphic correlation between the OSL, U-series, AMS ^{14}C and paleomagnetically dated boreholes from southern Changjiang delta plain. Boreholes FX and MFC are from Zhao et al. (2008). The codes from S1 to S5 represent the time of deposition from OIS 1 to OIS 5 for the strata. A significant incised valley occurred at FX and MFC during the lowstands of OIS 5d, 5b and 4, resulting in the thicker sedimentary succession deposited during S3.

Table 1

Lab code	Sample depth (m)	Dating material	Field water content (% dry mass)	γ dose rate [a] (Gy/ka^{-1})	β dose rate [b] (Gy/ka^{-1})	Cosmic-ray dose rate [c] (Gy/ka^{-1})	Total dose rate [d,e] (Gy/ka^{-1})	N / σ_d (%) [f]	D_e [g] (Gy)	Age [e,h] (ka)
UOW-313	11.4	Clayey silt	30	1.025±0.061	1.550±0.044	0.044±0.004	2.650±0.179	29 / 22.6±3.3	180±8	68±6
									*	*48±6
UOW-314	22.7	Clayey silt	35	1.064±0.063	1.482±0.072	0.019±0.002	2.594±0.174	28 / 20.6±3.6	190±9	73±6
UOW-315	28.3	Fine sand	25	0.875±0.051	1.231±0.060	0.015±0.002	2.151±0.149	26 / 13.2±2.8	215±7	100±8

[a] From x-ray fluorescence (XRF) (potassium) and thick-source alpha counter (TSAC) (uranium and thorium) measurements and adjusted for the field moisture content.

[b] From Geiger Müller beta counter (GMBC) measurements, corrected for beta-dose attenuation and adjusted for the field moisture content.

[c] From Prescott and Hutton (1994), assigned relative uncertainties of ± 10%, and adjusted for the field moisture content.

[d] Includes an assumed internal alpha dose rate of 0.03 ± 0.01 Gy/ka^{-1}.

[e] Mean ± total uncertainty (68% confidence interval), calculated as the quadratic sum of the random and systematic uncertainties.

[f] Number of aliquots used in the final D_e estimation (N) / relative standard deviation of D_e distribution after accounting for measurement uncertainties (overdispersion, σ_d).

[g] Central age model (CAM) (Galbraith *et al.*, 1999).

[h] Uncertainty includes a systematic component of ± 2% associated with laboratory beta-source calibration.

*Minimum Age Model (MAM) D_e and age (Galbraith *et al.*, 1999); an overdispersion value of 15% was added in quadrature to each of the D_e analytical uncertainties before analysis in the model.

Table 2

Core ID	Core depth (m)	Dating material	U (ppm)	Th (ppm)	K (%)	Dose rate (Gy/ka)	Equivalent dose (Gy)	OSL age (ka)	Lab. code
QP88	7.8	Clayey silt	3.02±0.4	12.6±1.3	1.54±0.1	3.23±0.34	216.92±17.97	67±9	L1032
	10.05	Silt	1.97 ±0.44	13.04±1.45	1.38±0.1	2.8±0.3	74.76±8.4	27±3	L770
	11.4	Silt	3.14 ±0.4	11.26 ±1.24	1.60±0.1	3.18±0.33	137.33±9.1	43±5	L1033
	22.25	Fine sand	2.01 ±0.32	9.15 ±1.08	1.58±0.1	2.6±0.3	161.94±15.6	61±6	L774
	22.9	Silt	2.16±0.04	9.41±0.03	1.81±0.02	2.9±0.2	222.08±10.15	77±7	L1035
	28.3	Clayey silt	3.07 ±0.39	9.54 ±1.30	1.43±0.1	2.8±0.3	221.52±22.5	78±9	L771
SG7	8.3	Silt	2.28	9.36	1.27	2.98	11.49	3.8±0.3	KSK001
	24.0	Silty clay	2.45	10.9	1.65	2.76	41.48	15.0±1.4	KSK002
	25.0	Stiff mud	3.42	11.8	1.59	3.49	63.55	18.2±1.6	KSK003
	40.5	Clayey silt	3.30	13.9	1.43	3.24	192.00	59.3±3.5	KSK004
	62.0	Clayey silt	2.70	12.3	1.81	3.32	228.85	69.0±5.1	KSK005
	63.0	Silty clay	3.56	14.8	2.43	3.67	272.32	74.2±2.5	KSK006
	80.8	Clayey silt	3.37	13.2	1.96	3.49	368.51	105.6±3.2	KSK007
	81.5	Clayey silt	3.18	15.4	1.87	2.53	298.92	118.2±11.1	KSK008
	101.0	Silty clay	2.19	11.0	1.13	3.48	515.59	148.1±6.5	KSK009

Table 3

Core depth (m)	Dating material	$\delta^{13}C$ (‰)	Conventional radiocarbon age (yr BP)	Calibrated age (cal yr BP; 2σ)	Lab. code
11.75	Shell	-3.9	41540±440	42970±720	Beta-309663
14.2	Shell	-1.8	43050±510	44480±1270	Beta-309664

Table 4

Core ID	Core depth (m)	Dating material		U (ppm)	Th (ppm)	$^{234}U/^{238}U$	$^{230}Th/^{232}Th$	$^{230}Th/^{234}U$	Corrected $^{234}U/^{238}U$	Corrected $^{230}Th/^{234}U$	Age (ka)
QP88	22	Shell		0.541±0.022		1.480±0.074	23.416	0.480±0.025			68.2±4.7
	29.2	Shell		0.212±0.012		1.304±0.064	70.34	0.529±0.016			79.1±3.2
	48	Shell		0.463±0.023		1.659±0.102	18.381	0.756±0.035			134.1±11.1
SG7	52.7*	Carbonate separated from sediment	a	0.439±0.032	1.591±0.064	1.710±0.150	0.668±0.042	0.473±0.035	1.714±0.075	0.351±0.025	45.3±3.7
			b	0.825±0.055	3.949±0.176	1.723±0.140	0.546±0.039	0.504±0.038			
			c	0.804±0.035	3.609±0.104	1.676±0.089	0.576±0.026	0.512±0.025			
	65.75	Shell		2.567±0.126	-	2.095±0.115	188.47	0.462±0.023	-	-	63.0±3.6
	72.4	Shell		0.226±0.014	-	2.148±0.164	19.03	0.579±0.052	-	-	85.9+6.1

*The carbonate-rich sediment at core depth 52.7 m from SG7 was separated into three particle sizes (a, <0.063 μm; b, 0.063–0.125 μm; c, >0.125 μm) by sieving before specimen preparation and measurement. Concentrations of U and Th and their isotopes were measured for all three components before calculating the corrected isotope ratios of $^{234}U/^{238}U$ and $^{230}Th/^{234}U$.

Table 5

Core depth (m)	Intertidal beach	Freshwater	Shallow marine	Unit
20.8	*Umbonium* sp.; *Nassarius* (Phrontis) *caelatulus* Wang; *Assiminea cf. colombeliana* Heude			S5-1
21	*Umbonium thomasi* (Crosse); *Nassarius* (Phrontis) *caelatulus* Wang			
22.15	*Cerithidea* sp.; *Umbonium thomasi* (Crosse)			
29.2			*Mitrella* sp.	
49.7		*Bellamya* sp.		S5-2

Table 6

Core depth (m)	Estuary	Fresh to brackish water	Unit
20.8	*Silqua mimima* (Gmelin)	*Corbicula leana* Prime; *Corbicula largillerti* (Philippi)	S5-1
21	*Potamocorbula amurensis* (Schrenck)	*Corbicula leana* Prime	
22.15	*Potamocorbula amurensis* (Schrenck)	*Corbicula leana* Prime	
29.2	*Potamocorbula amurensis* (Schrenck); *Ostrea* sp.	*Corbicula leana* Prime	
48		*Corbicula leana* Prime; *Corbicula largillerti* (Philippi)	S5-2
49.7		*Corbicula leana* Prime	

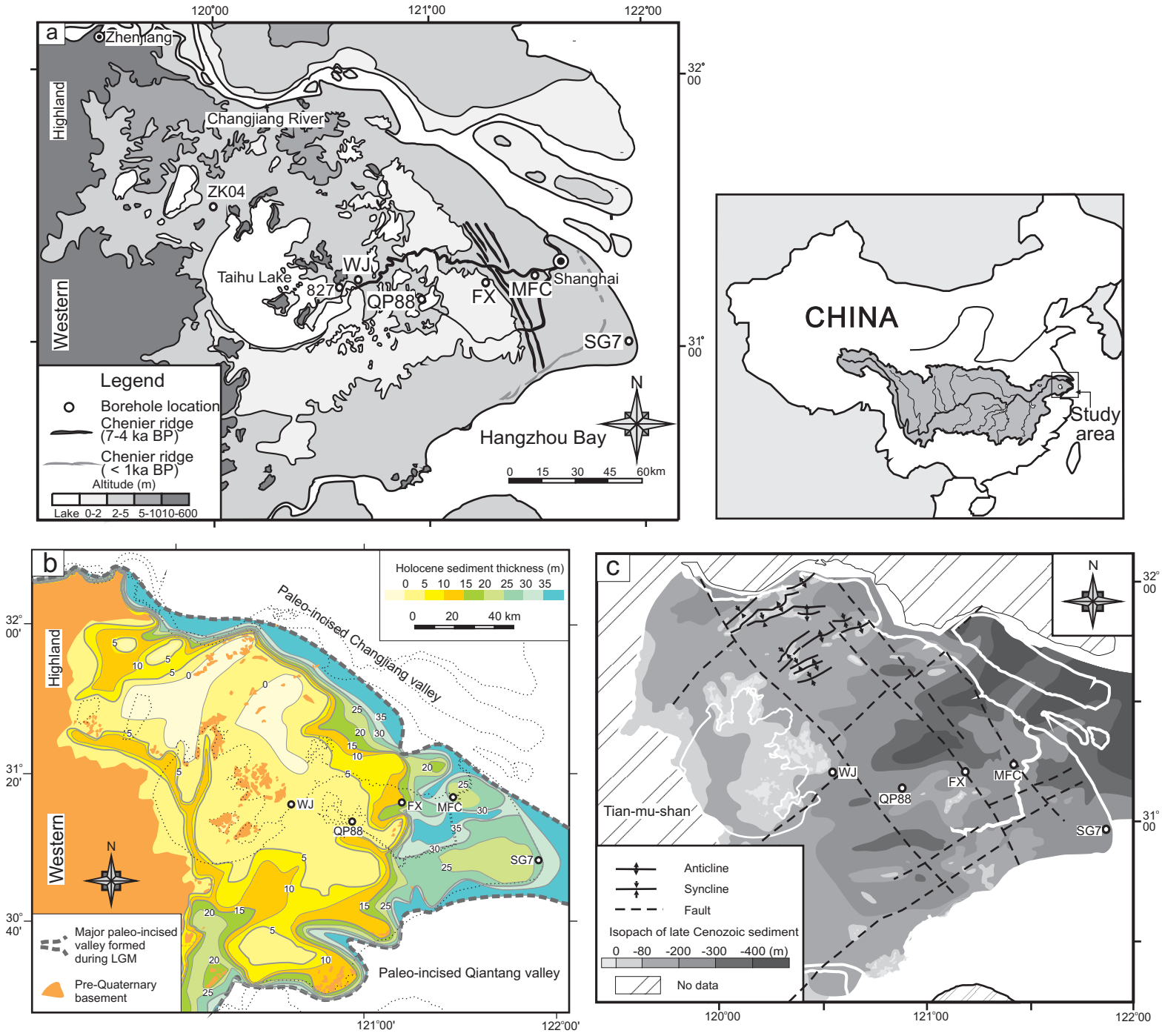
a
Zhenjiang
Highland
Changjiang River
ZK04
Taihu Lake
WJ
827
QP88
FX
MFC
Shanghai
SG7
Western
Hangzhou Bay
N
0 15 30 45 60km
120°00
121°00
122°00
32° 00
31° 00
Legend
Borehole location
Chenier ridge (7-4 ka BP)
Chenier ridge (< 1ka BP)
Altitude (m)
Lake 0-2 2-5 5-10 10-60
CHINA
Study area
b
Holocene sediment thickness (m)
0 5 10 15 20 25 30 35
0 20 40 km
Paleo-incised Changjiang valley
Highland
Western
Major paleo-incised valley formed during LGM
Pre-Quaternary basement
Paleo-incised Qiantang valley
32° 00'
31° 20'
30° 40'
121°00'
122°00'
c
Tian-mu-shan
Anticline
Syncline
Fault
Isopach of late Cenozoic sediment
0 -80 -200 -300 -400 (m)
No data
120°00
121°00
122°00
32° 00
31° 00

Figure 1

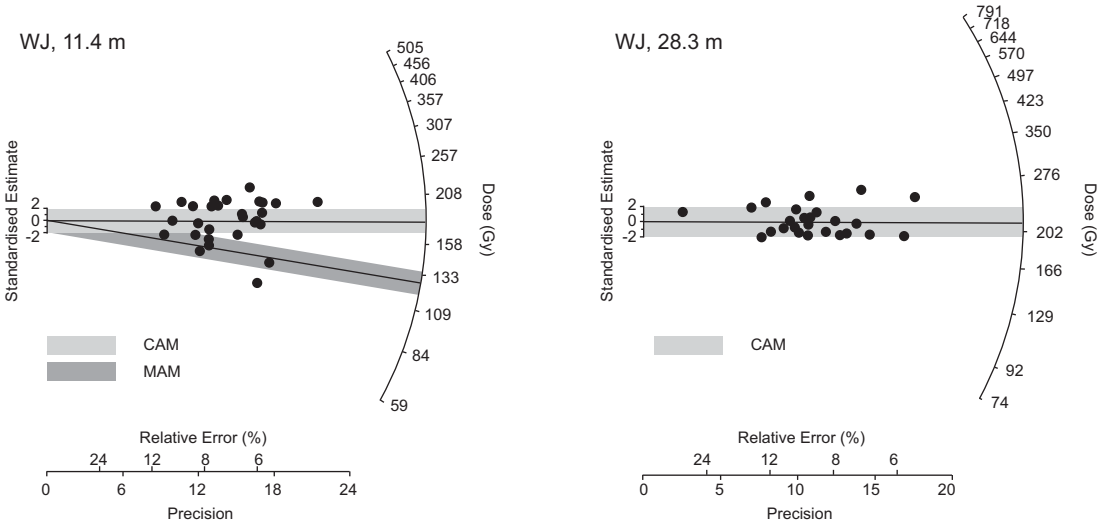
WJ, 11.4 m
Standardised Estimate
2
0
-2
CAM
MAM
505
456
406
357
307
257
208
158
133
109
84
59
Dose (Gy)
Relative Error (%)
24
12
8
6
0
6
12
18
24
Precision
WJ, 28.3 m
Standardised Estimate
2
0
-2
CAM
791
718
644
570
497
423
350
276
202
166
129
92
74
Dose (Gy)
Relative Error (%)
24
12
8
6
0
5
10
15
20
Precision

Figure 2

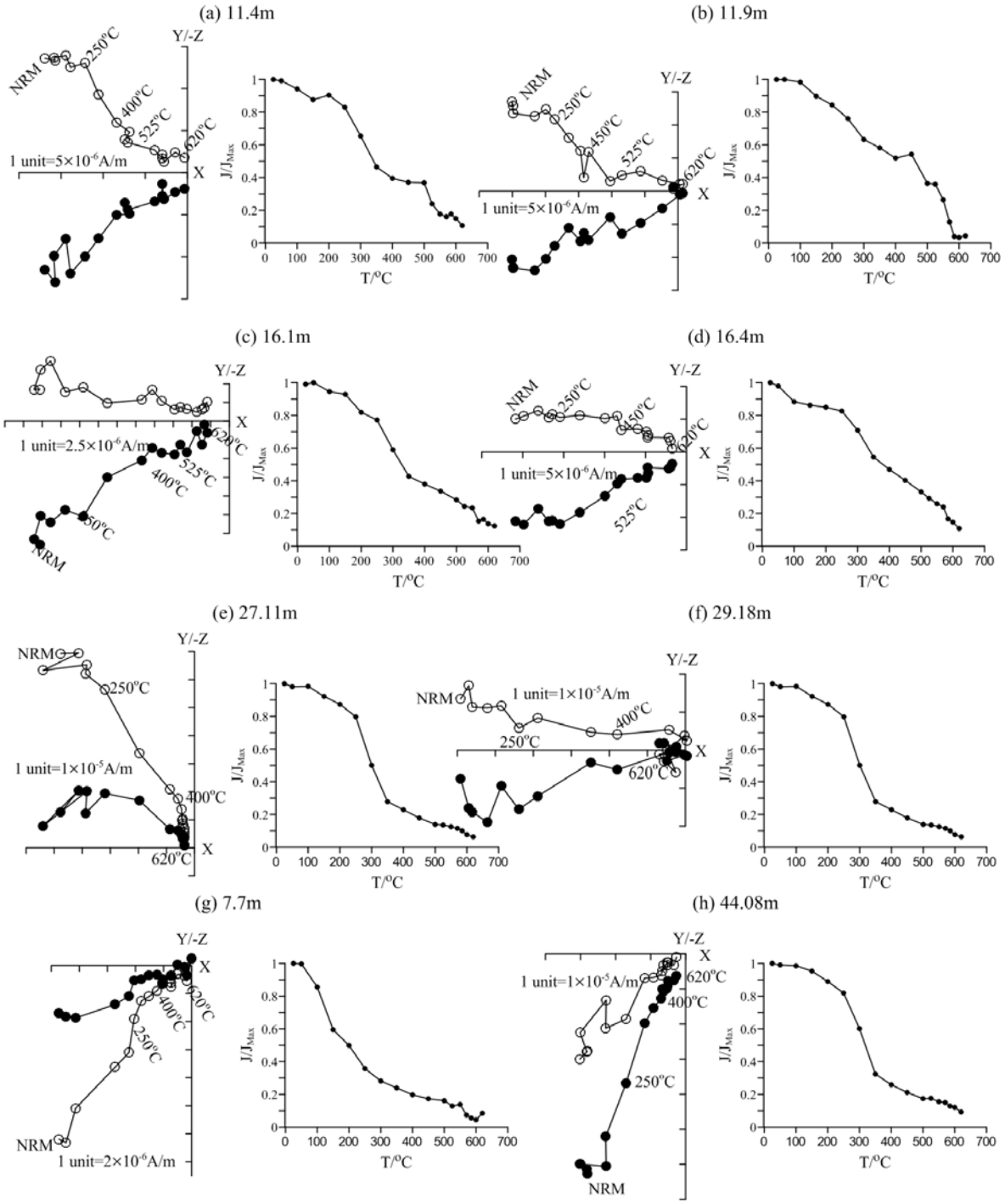
(a) 11.4m
(b) 11.9m
(c) 16.1m
(d) 16.4m
(e) 27.11m
(f) 29.18m
(g) 7.7m
(h) 44.08m
Y/-Z
X
NRM
250°C
400°C
525°C
620°C
450°C
50°C
1 unit=5×10⁻⁶A/m
1 unit=2.5×10⁻⁶A/m
1 unit=1×10⁻⁵A/m
1 unit=2×10⁻⁶A/m
J/J_Max
T/°C

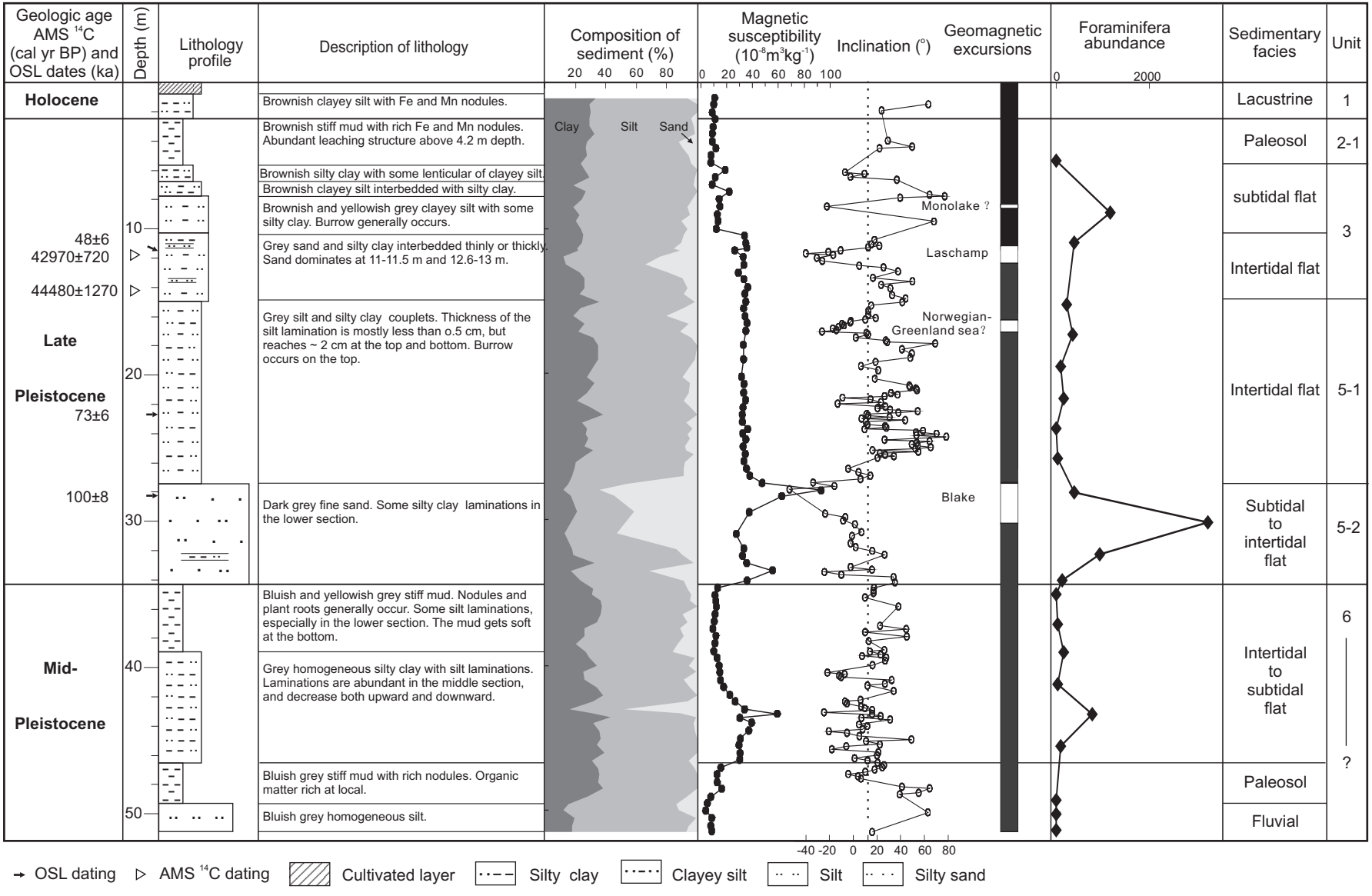
Geologic age AMS 14C (cal yr BP) and OSL dates (ka)
Depth (m)
Lithology profile
Description of lithology
Composition of sediment (%)
Magnetic susceptibility (10-8m3kg-1)
Inclination (°)
Geomagnetic excursions
Foraminifera abundance
Sedimentary facies
Unit
Holocene
Brownish clayey silt with Fe and Mn nodules.
Lacustrine
1
Brownish stiff mud with rich Fe and Mn nodules. Abundant leaching structure above 4.2 m depth.
Paleosol
2-1
Brownish silty clay with some lenticular of clayey silt.
Brownish clayey silt interbedded with silty clay.
Brownish and yellowish grey clayey silt with some silty clay. Burrow generally occurs.
subtidal flat
3
48±6
42970±720
44480±1270
Grey sand and silty clay interbedded thinly or thickly. Sand dominates at 11-11.5 m and 12.6-13 m.
Intertidal flat
Late
Pleistocene
73±6
Grey silt and silty clay couplets. Thickness of the silt lamination is mostly less than o.5 cm, but reaches ~ 2 cm at the top and bottom. Burrow occurs on the top.
Intertidal flat
5-1
100±8
Dark grey fine sand. Some silty clay laminations in the lower section.
Subtidal to intertidal flat
5-2
Bluish and yellowish grey stiff mud. Nodules and plant roots generally occur. Some silt laminations, especially in the lower section. The mud gets soft at the bottom.
6
Mid-
Pleistocene
Grey homogeneous silty clay with silt laminations. Laminations are abundant in the middle section, and decrease both upward and downward.
Intertidal to subtidal flat
Bluish grey stiff mud with rich nodules. Organic matter rich at local.
Paleosol
?
Bluish grey homogeneous silt.
Fluvial
Clay
Silt
Sand
Monolake ?
Laschamp
Norwegian-Greenland sea?
Blake
OSL dating
AMS 14C dating
Cultivated layer
Silty clay
Clayey silt
Silt
Silty sand

Figure 4

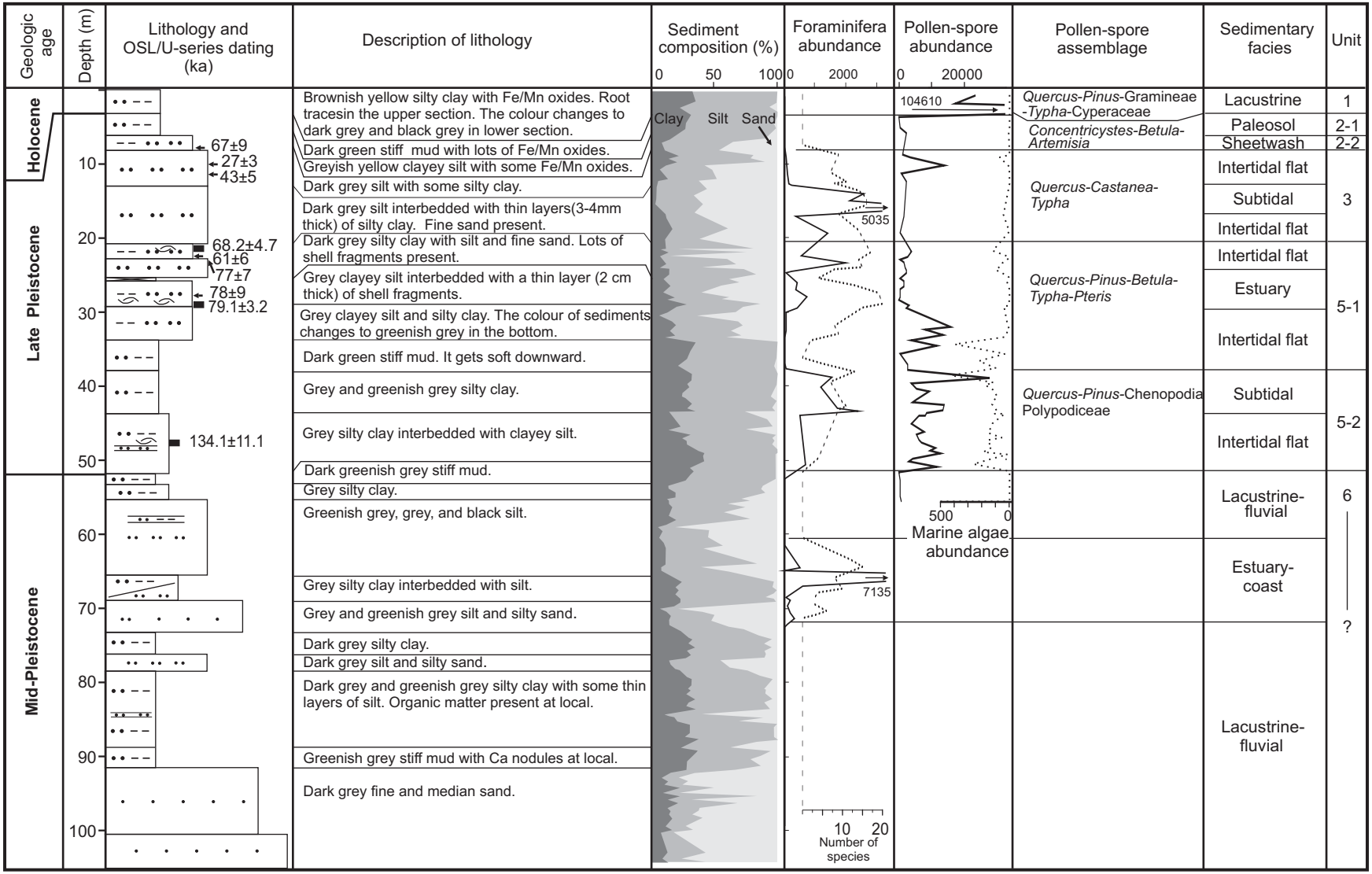
Geologic age
Depth (m)
Lithology and OSL/U-series dating (ka)
Description of lithology
Sediment composition (%)
Foraminifera abundance
Pollen-spore abundance
Pollen-spore assemblage
Sedimentary facies
Unit
Holocene
Late Pleistocene
Mid-Pleistocene
67±9
27±3
43±5
68.2±4.7
61±6
77±7
78±9
79.1±3.2
134.1±11.1
Brownish yellow silty clay with Fe/Mn oxides. Root tracesin the upper section. The colour changes to dark grey and black grey in lower section.
Dark green stiff mud with lots of Fe/Mn oxides.
Greyish yellow clayey silt with some Fe/Mn oxides.
Dark grey silt with some silty clay.
Dark grey silt interbedded with thin layers(3-4mm thick) of silty clay. Fine sand present.
Dark grey silty clay with silt and fine sand. Lots of shell fragments present.
Grey clayey silt interbedded with a thin layer (2 cm thick) of shell fragments.
Grey clayey silt and silty clay. The colour of sediments changes to greenish grey in the bottom.
Dark green stiff mud. It gets soft downward.
Grey and greenish grey silty clay.
Grey silty clay interbedded with clayey silt.
Dark greenish grey stiff mud.
Grey silty clay.
Greenish grey, grey, and black silt.
Grey silty clay interbedded with silt.
Grey and greenish grey silt and silty sand.
Dark grey silty clay.
Dark grey silt and silty sand.
Dark grey and greenish grey silty clay with some thin layers of silt. Organic matter present at local.
Greenish grey stiff mud with Ca nodules at local.
Dark grey fine and median sand.
Clay
Silt
Sand
104610
5035
7135
Number of species
Marine algae abundance
Quercus-Pinus-Gramineae-Typha-Cyperaceae
Concentricystes-Betula-Artemisia
Quercus-Castanea-Typha
Quercus-Pinus-Betula-Typha-Pteris
Quercus-Pinus-Chenopodia Polypodiceae
Lacustrine
Paleosol
Sheetwash
Intertidal flat
Subtidal
Estuary
Lacustrine-fluvial
Estuary-coast
1
2-1
2-2
3
5-1
5-2
6
?
OSL dating
U-series dating
Cultivated layer
Silty clay
Clayey silt
Silty sand
Fine sand
Gravelly sand

Figure 5

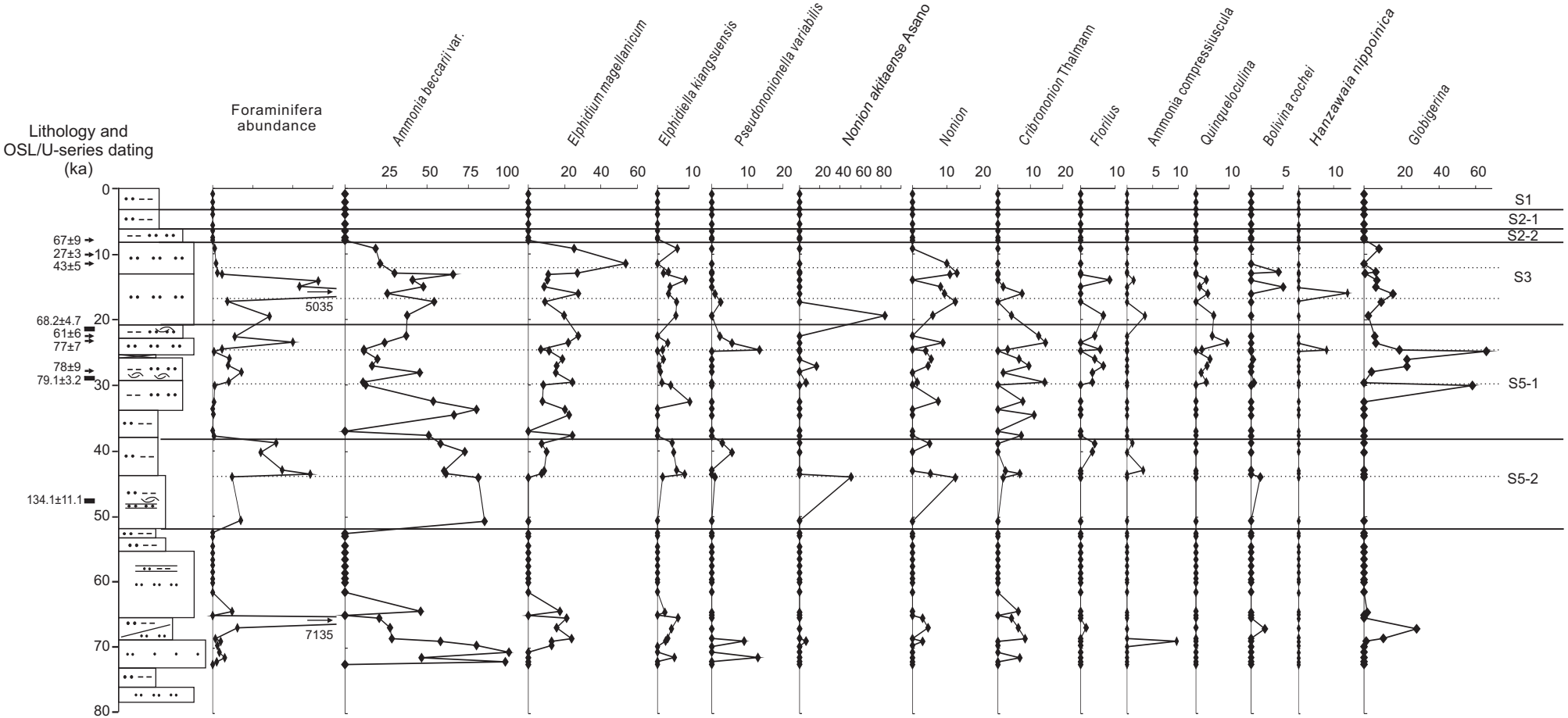
Lithology and
OSL/U-series dating
(ka)
Foraminifera
abundance
Ammonia beccarii var.
Elphidium magellanicum
Elphidiella kiangsuensis
Pseudononionella variabilis
Nonion akitaense Asano
Nonion
Cribrononion Thalmann
Florilus
Ammonia compressiuscula
Quinqueloculina
Bolivina cochei
Hanzawaia nippoinica
Globigerina
0
10
20
30
40
50
60
70
80
67±9
27±3
43±5
68.2±4.7
61±6
77±7
78±9
79.1±3.2
134.1±11.1
5035
7135
S1
S2-1
S2-2
S3
S5-1
S5-2

Figure 6

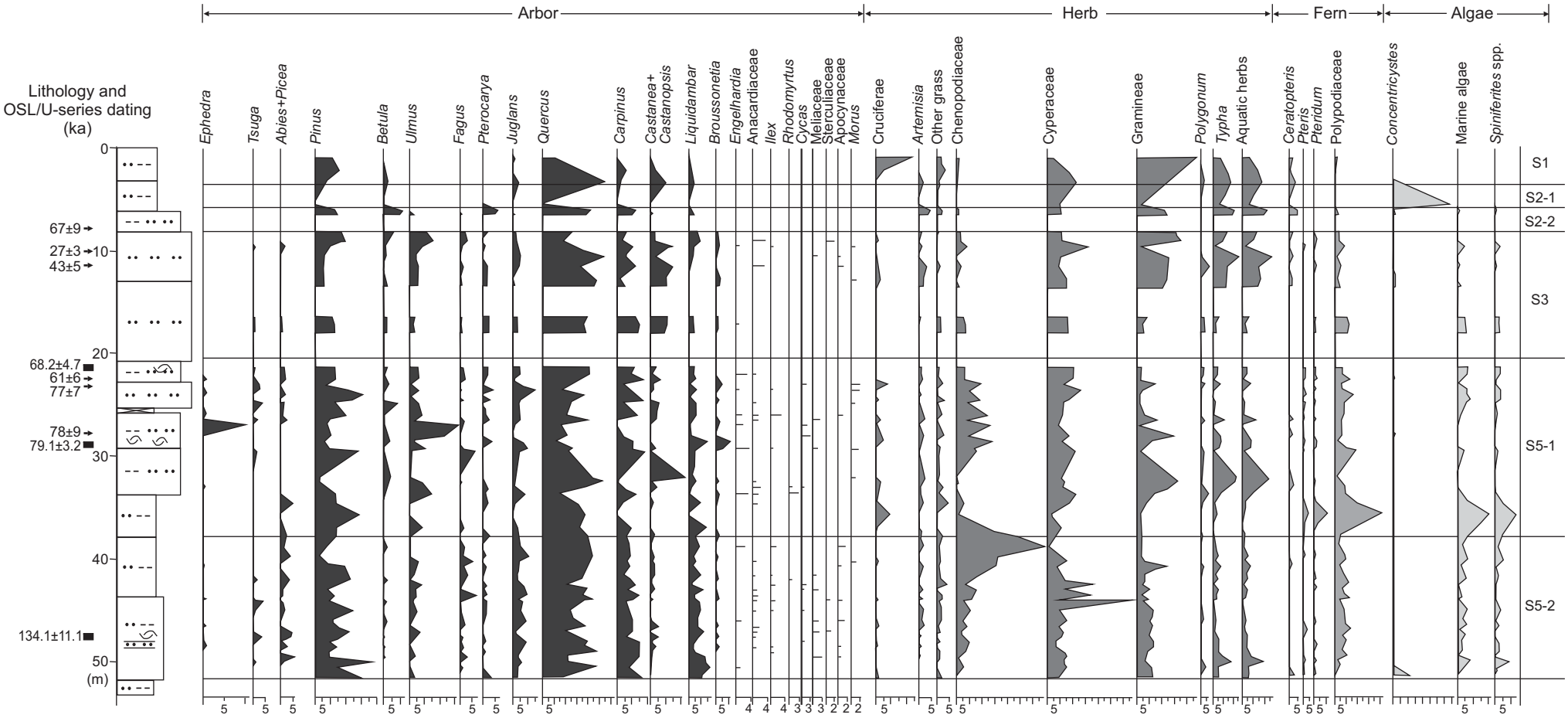
Lithology and
OSL/U-series dating
(ka)
0
10
20
30
40
50
(m)
67±9
27±3
43±5
68.2±4.7
61±6
77±7
78±9
79.1±3.2
134.1±11.1
Arbor
Herb
Fern
Algae
Ephedra
Tsuga
Abies+Picea
Pinus
Betula
Ulmus
Fagus
Pterocarya
Juglans
Quercus
Carpinus
Castanea+
Castanopsis
Liquidambar
Broussonetia
Engelhardia
Anacardiaceae
Ilex
Rhodomyrtus
Cycas
Meliaceae
Sterculiaceae
Apocynaceae
Morus
Cruciferae
Artemisia
Other grass
Chenopodiaceae
Cyperaceae
Gramineae
Polygonum
Typha
Aquatic herbs
Ceratopteris
Pteris
Pteridium
Polypodiaceae
Concentricystes
Marine algae
Spiniferites spp.
S1
S2-1
S2-2
S3
S5-1
S5-2

Figure 7

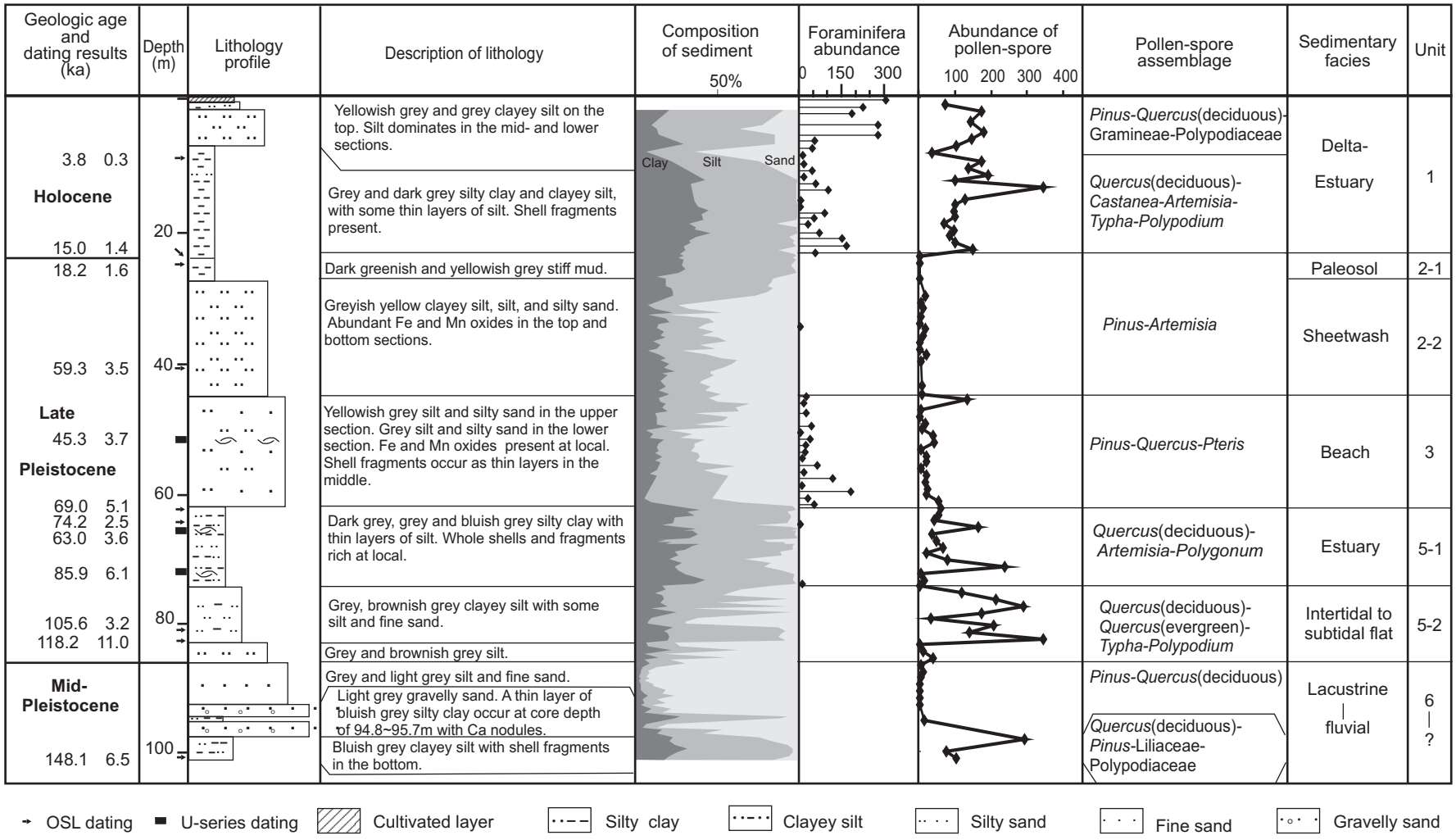
Geologic age and dating results (ka)
Depth (m)
Lithology profile
Description of lithology
Composition of sediment
50%
Clay
Silt
Sand
Foraminifera abundance
0 150 300
Abundance of pollen-spore
100 200 300 400
Pollen-spore assemblage
Sedimentary facies
Unit
3.8 0.3
Holocene
15.0 1.4
18.2 1.6
59.3 3.5
Late
45.3 3.7
Pleistocene
69.0 5.1
74.2 2.5
63.0 3.6
85.9 6.1
105.6 3.2
118.2 11.0
Mid-Pleistocene
148.1 6.5
20
40
60
80
100
Yellowish grey and grey clayey silt on the top. Silt dominates in the mid- and lower sections.
Grey and dark grey silty clay and clayey silt, with some thin layers of silt. Shell fragments present.
Dark greenish and yellowish grey stiff mud.
Greyish yellow clayey silt, silt, and silty sand. Abundant Fe and Mn oxides in the top and bottom sections.
Yellowish grey silt and silty sand in the upper section. Grey silt and silty sand in the lower section. Fe and Mn oxides present at local. Shell fragments occur as thin layers in the middle.
Dark grey, grey and bluish grey silty clay with thin layers of silt. Whole shells and fragments rich at local.
Grey, brownish grey clayey silt with some silt and fine sand.
Grey and brownish grey silt.
Grey and light grey silt and fine sand.
Light grey gravelly sand. A thin layer of bluish grey silty clay occur at core depth of 94.8~95.7m with Ca nodules.
Bluish grey clayey silt with shell fragments in the bottom.
Pinus-Quercus(deciduous)-Gramineae-Polypodiaceae
Quercus(deciduous)-Castanea-Artemisia-Typha-Polypodium
Pinus-Artemisia
Pinus-Quercus-Pteris
Quercus(deciduous)-Artemisia-Polygonum
Quercus(deciduous)-Quercus(evergreen)-Typha-Polypodium
Pinus-Quercus(deciduous)
Quercus(deciduous)-Pinus-Liliaceae-Polypodiaceae
Delta-Estuary
Paleosol
Sheetwash
Beach
Estuary
Intertidal to subtidal flat
Lacustrine | fluvial
1
2-1
2-2
3
5-1
5-2
6 | ?
OSL dating
U-series dating
Cultivated layer
Silty clay
Clayey silt
Silty sand
Fine sand
Gravelly sand

Figure 8

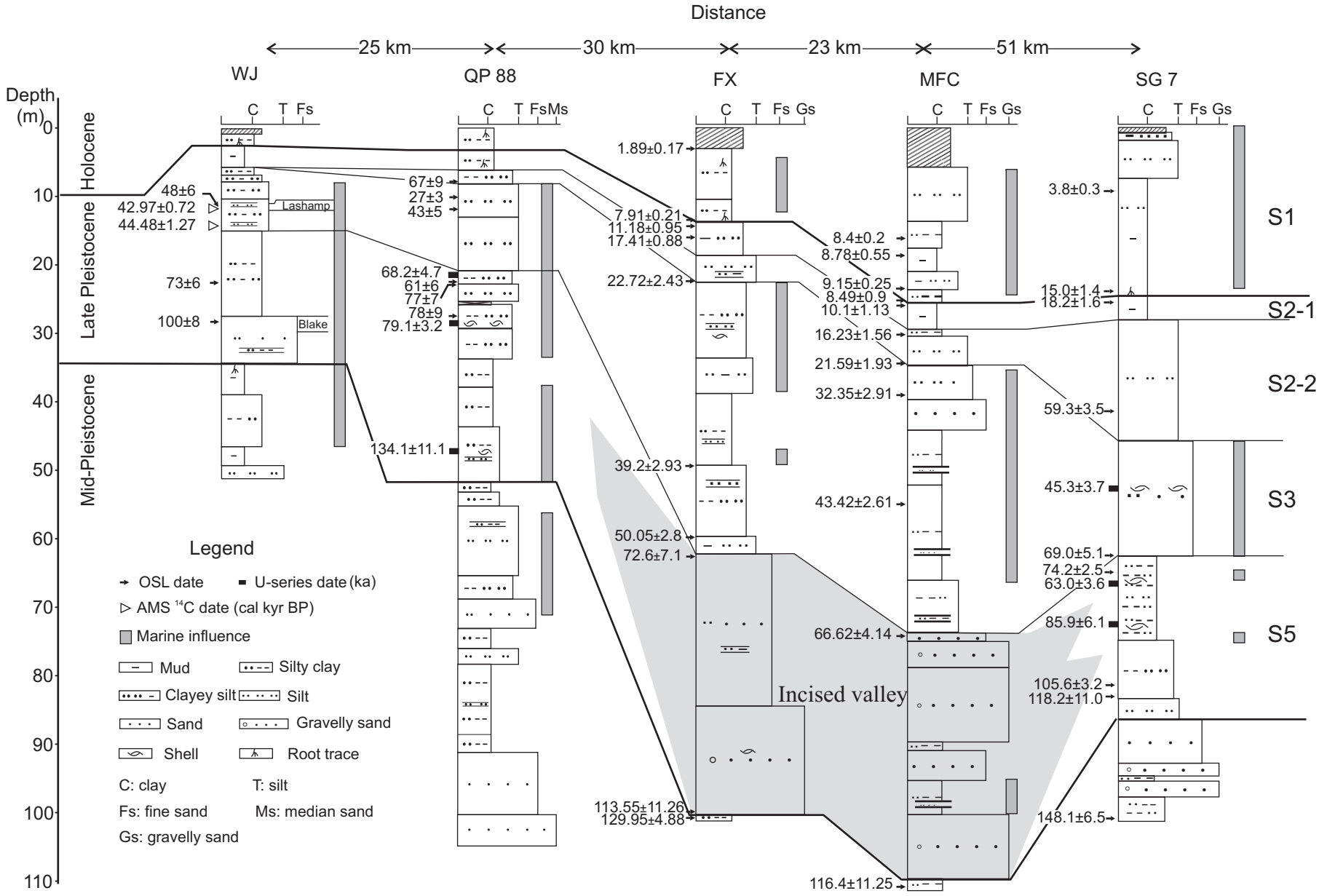
Distance
25 km
30 km
23 km
51 km
WJ
QP 88
FX
MFC
SG 7
C T Fs
C T FsMs
C T Fs Gs
Depth (m)
Holocene
Late Pleistocene
Mid-Pleistocene
Lashamp
Blake
48±6
42.97±0.72
44.48±1.27
73±6
100±8
67±9
27±3
43±5
68.2±4.7
61±6
77±7
78±9
79.1±3.2
134.1±11.1
1.89±0.17
7.91±0.21
11.18±0.95
17.41±0.88
22.72±2.43
39.2±2.93
50.05±2.8
72.6±7.1
113.55±11.26
129.95±4.88
8.4±0.2
8.78±0.55
9.15±0.25
8.49±0.9
10.1±1.13
16.23±1.56
21.59±1.93
32.35±2.91
43.42±2.61
66.62±4.14
116.4±11.25
3.8±0.3
15.0±1.4
18.2±1.6
59.3±3.5
45.3±3.7
69.0±5.1
74.2±2.5
63.0±3.6
85.9±6.1
105.6±3.2
118.2±11.0
148.1±6.5
S1
S2-1
S2-2
S3
S5
Incised valley
Legend
OSL date
U-series date (ka)
AMS 14C date (cal kyr BP)
Marine influence
Mud
Silty clay
Clayey silt
Silt
Sand
Gravelly sand
Shell
Root trace
C: clay
T: silt
Fs: fine sand
Ms: median sand
Gs: gravelly sand

Figure 9